9 SCIENTIFIC HIGHLIGHT OF THE MONTH

Realistic investigations of correlated electron systems with LDA+DMFT

K. Held[1], I. A. Nekrasov[2], G. Keller[3], V. Eyert[4], N. Blümer[5], A. K. McMahan[6], R. T. Scalettar[7], Th. Pruschke[3], V. I. Anisimov[2], and D. Vollhardt[3]

[1] *Max-Planck Institute for Solid State Research, D-70569 Stuttgart, Germany*

[2] *Institute of Metal Physics, Russian Academy of Sciences-Ural Division, Yekaterinburg GSP-170, Russia*

[3] *Theoretical Physics III, Center for Electronic Correlations and Magnetism, Institute for Physics, University of Augsburg, D-86135 Augsburg, Germany*

[4] *Institute for Physics, Theoretical Physics II, University of Augsburg, D-86135 Augsburg, Germany*

[5] *Institute for Physics, Johannes Gutenberg University, D-55099 Mainz, Germany*

[6] *Lawrence Livermore National Laboratory, University of California, Livermore, CA 94550, USA*

[7] *Physics Department, University of California, Davis, CA 95616, USA*

Abstract

Conventional band structure calculations in the local density approximation (LDA)[1–3] are highly successful for many materials, but miss important aspects of the physics and energetics of strongly correlated electron systems, such as transition metal oxides and f-electron systems displaying, e.g., Mott insulating and heavy quasiparticle behavior. In this respect, the LDA+DMFT approach which merges LDA with a modern many-body approach, the dynamical mean-field theory (DMFT) has proved to be a breakthrough for the realistic modeling of correlated materials. Depending on the strength of the electronic correlation, a LDA+DMFT calculation yields the weakly correlated LDA results, a strongly correlated metal, or a Mott insulator. In this paper, the basic ideas and the set-up of the LDA+DMFT(X) approach, where X is the method used to solve the DMFT equations, are discussed. Results obtained with X=QMC (quantum Monte Carlo) and X=NCA (non-crossing approximation) are presented and compared, showing that the method X matters quantitatively. We also discuss LDA+DMFT results for two prime examples of correlated materials, i.e., V_2O_3 and Ce which undergo a Mott-Hubbard metal-insulator and volume collapse transition, respectively.

Table of contents

1 Introduction

One of the most important challenges of theoretical solid state physics is the development of tools for the accurate calculation of material properties. In this respect, density functional theory (DFT) within the local density approximation (LDA)[1–3] turned out to be unexpectedly successful, and established itself as *the* method for realistic solid state calculations in the last century. This is surprising because LDA is a serious approximation to the Coulomb interaction between electrons. In particular the correlation but also the exchange contribution of the Coulomb interaction is only treated rudimentarily, i.e., by means of a *local* density and by a functional obtained from the jellium model, a weakly correlated problem. The success of LDA shows, however, that this treatment is sufficient for many materials, both for calculating ground state energies and bandstructures, implying that electronic correlations are rather weak in these materials. However, there are important classes of materials where LDA fails, such as transition metal oxides or heavy fermion systems, i.e., materials where electronic correlations are strong. For example, LDA predicts La_2CuO_4 and V_2O_3, to be metals[4,5] whereas, in reality, they are insulators. The physics of these Mott insulators is dominated by the formation of Hubbard bands, an effect of electronic correlations which splits the LDA bands into two sets of bands, separated by a local Coulomb repulsion U. Such Mott insulating behavior occurs already in the paramagnetic phase, with magnetic order setting in at lower temperatures. The Mott physics and the associated energy gain is completely missing in the LDA. It can, however, be described by the LDA+U method, at least for ordered systems. But, the energy gain due to the formation of Hubbard bands is so large in LDA+U that for realistic values of U it almost automatically yields split bands and (ordered) insulating behavior, even if this is not correct. The reason for this is that the energy of the correlated metal is strongly overestimated. Hence, LDA+U is a

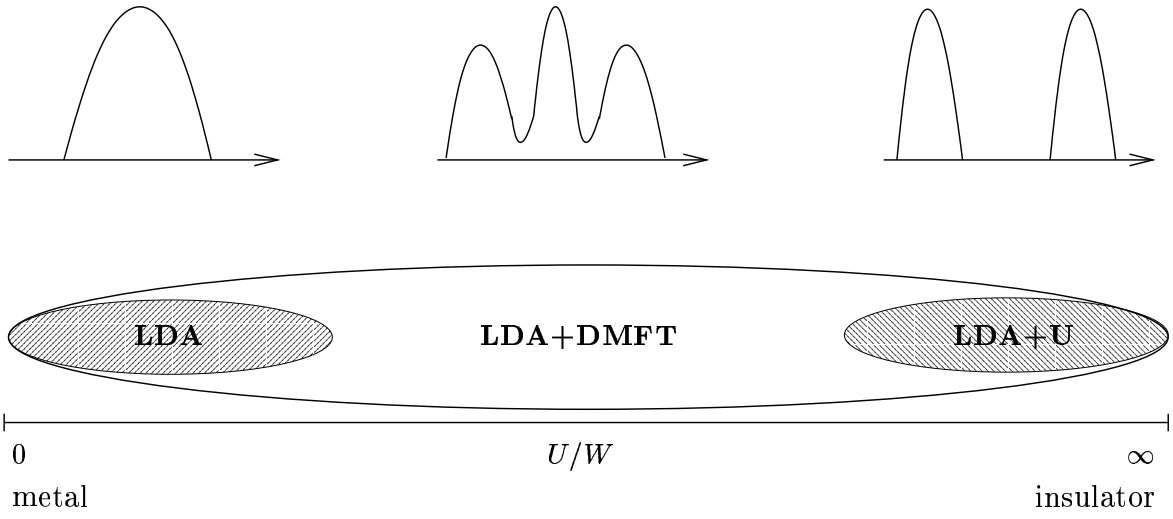

Figure 1: With increasing strength of the local Coulomb repulsion U (relative to the LDA bandwidth W), one observes a weakly correlated metal (left density of states), a strongly correlated metal with a quasiparticle peak at the Fermi energy (middle), and a Mott insulator (right). The weakly correlated metal and the (ordered) Mott insulator are correctly described by LDA and LDA+U, respectively. LDA+DMFT gives the correct answer for all values of U and subsumes the LDA valid for small U/W and the LDA+U results for the Mott insulator appearing at large U/W.

good method for describing Mott insulators, but not for calculating strongly correlated metals or systems in the vicinity of a Mott-Hubbard metal-insulator transition. Missing in both LDA and LDA+U is the *quasiparticle physics*, which even at a rather large Coulomb interaction U (or at $U = \infty$ with a non-integer number of interacting electrons per site) still gives a metallic behavior determined by quasiparticles with a larger effective mass than the LDA electrons. This mass enhancement ranges from a moderate increase in many transition metal oxides to the high effective masses observed in $4f$-based heavy fermion compounds. LDA and also LDA+U fail to account for this kind of physics and the associated Kondo-like energy scale gained in comparison with the Mott insulator.

LDA+DMFT does not only include the correct quasiparticle physics and the corresponding energetics but, at the same time, reproduces the LDA and LDA+U results in the limits where these methods are valid, see Fig. 1. For weakly correlated systems, we know that LDA provides the correct description, as does the LDA+DMFT approach which gives the same results as LDA if the local Coulomb interaction U is small. On the other hand, LDA+DMFT agrees with the LDA+U results for symmetry-broken Mott insulators at large Coulomb interaction U. In addition, however, LDA+DMFT also describes the correlated metals occurring either at somewhat smaller Coulomb interactions U *or* when Mott insulators are doped. Thus, LDA+DMFT provides the correct physics for all Coulomb interactions and dopings, whereas LDA yields an uncorrelated metal even if the material at hand is a strongly-correlated metal or a Mott insulator. Similarly, LDA+U yields an insulator for the *ab-initio*-calculated U-values of 3d transition metal oxides, even for materials which should be metallic.

With the ability of LDA+DMFT to describe the full range of materials from weakly to strongly correlated metals to Mott insulators, it is not astonishing that it has proved to be a breakthrough for the calculation of correlated materials. Since more and more physicists from the bandstructure and many-body communities show interest in this novel method, we would like to present here, as a ψ_k scientific highlight of the month, an introduction to LDA+DMFT. We also present results for two of the most famous strongly-correlated materials, i.e., the transition metal oxide V_2O_3 which is the prime example of a system undergoing a Mott-Hubbard metal-insulator transition, and the $4f$-electron system Ce with its volume collapse transition. The presentation is following in many parts the conference proceedings Ref. 6, also see the conference proceedings Refs. 7.

In Section 2 the LDA+DMFT approach is presented, starting with the *ab initio* electronic Hamiltonian in Section 2.1, continuing with DFT in Section 2.2, LDA in Section 2.3, the construction of a model Hamiltonian in Section 2.4, and DMFT in Section 2.5. As methods used to solve the DMFT we discuss the quantum Monte Carlo (QMC) algorithm in Section 2.6 and the non-crossing approximation (NCA) in Section 2.7. A simplified treatment for transition metal oxides is introduced in Section 2.8. Extensions and alternatives to the LDA+DMFT approach are discussed, focusing on a self-consistent LDA+DMFT scheme in Section 3.1, spectral density functional theory in Section 3.2, cluster extensions of DMFT in Section 3.3, and the GW+DMFT approach in Section 3.4. As a particular example, the LDA+DMFT calculation for $La_{1-x}Sr_xTiO_3$ is discussed in Section 4, emphasizing that the method X to solve the DMFT matters on a quantitative level. Our calculations for the Mott-Hubbard metal-insulator transition in V_2O_3 are presented in Section 5, in comparison to the experiment. Section 6 reviews our recent calculations of the Ce α-γ transition, in the perspective of the models referred to as Kondo volume collapse and Mott transition scenario. A summary of the LDA+DMFT set-up and applications followed by a discussion of future prospects closes the presentation in Section 7.

2 The LDA+DMFT approach

2.1 Ab initio electronic Hamiltonian

Within Born-Oppenheimer approximation[8] and neglecting relativistic effects, electronic properties of solid state systems are described by the electronic Hamiltonian

$$\begin{aligned} \hat{H} &= \sum_\sigma \int d^3r\ \hat{\Psi}^+(\mathbf{r},\sigma)\left[-\frac{\hbar^2}{2m_e}\Delta + V_{\rm ion}(\mathbf{r})\right]\hat{\Psi}(\mathbf{r},\sigma) \\ &\quad + \frac{1}{2}\sum_{\sigma\sigma'}\int d^3r\, d^3r'\ \hat{\Psi}^+(\mathbf{r},\sigma)\hat{\Psi}^+(\mathbf{r}',\sigma')\ V_{\rm ee}(\mathbf{r}-\mathbf{r}')\ \hat{\Psi}(\mathbf{r}',\sigma')\hat{\Psi}(\mathbf{r},\sigma). \end{aligned} \tag{1}$$

Here, $\hat{\Psi}^+(\mathbf{r},\sigma)$ and $\hat{\Psi}(\mathbf{r},\sigma)$ are field operators that create and annihilate an electron at position $\mathbf{r}$ with spin σ, Δ is the Laplace operator, m_e the electron mass, e the electron charge, and

$$V_{\rm ion}(\mathbf{r}) = -e^2\sum_i \frac{Z_i}{|\mathbf{r}-\mathbf{R_i}|} \quad \text{and} \quad V_{\rm ee}(\mathbf{r}-\mathbf{r}') = \frac{e^2}{2}\sum_{\mathbf{r}\neq\mathbf{r}'}\frac{1}{|\mathbf{r}-\mathbf{r}'|} \tag{2}$$

denote the one-particle ionic potential of all ions i with charge eZ_i at given positions $\mathbf{R_i}$, and the electron-electron interaction, respectively.

While the *ab initio* Hamiltonian (1) is easy to write down it is impossible to solve it exactly if more than a few electrons are involved. Numerical methods like Green's Function Monte Carlo and related approaches have been used successfully for relatively modest numbers of electrons. Even so, however, the focus of the work has been on jellium and on light atoms and molecules like H, H_2, ^{3}He, ^{4}He with only a few electrons. Because of this, one has to make substantial approximations to deal with the Hamiltonian (1) like the LDA approximation or the LDA+DMFT approach which is the subject of the present paper.

2.2 Density functional theory

The fundamental theorem of DFT by Hohenberg and Kohn[1] (see, e.g., the review by Jones and Gunnarsson[3]) states that the ground state energy is a functional of the electron density which assumes its minimum at the electron density of the ground state. Following Levy,[9] this theorem is easily proved and the functional even constructed by taking the minimum (infimum) of the energy expectation value w.r.t. all (many-body) wave functions $\varphi(\mathbf{r_1}\sigma_1, ...\, \mathbf{r_N}\sigma_N)$ at a given electron number N which yield the electron density $\rho(\mathbf{r})$:

$$E[\rho] = \inf\Big\{\langle\varphi|\hat{H}|\varphi\rangle \;\Big|\; \langle\varphi|\sum_{i=1}^{N}\delta(\mathbf{r}-\mathbf{r_i})|\varphi\rangle = \rho(\mathbf{r})\Big\}. \tag{3}$$

However, this construction is of no practical value since it actually requires the evaluation of the Hamiltonian (1). Only certain contributions like the Hartree energy, i.e., $E_{\rm Hartree}[\rho] = \frac{1}{2}\int d^3r'\, d^3r\; V_{\rm ee}(\mathbf{r}-\mathbf{r'})\;\rho(\mathbf{r'})\rho(\mathbf{r})$, and the energy of the ionic potential $E_{\rm ion}[\rho] = \int d^3r\; V_{\rm ion}(\mathbf{r})\;\rho(\mathbf{r})$ can be expressed directly in terms of the electron density. This leads to

$$E[\rho] = E_{\rm kin}[\rho] + E_{\rm ion}[\rho] + E_{\rm Hartree}[\rho] + E_{\rm xc}[\rho], \tag{4}$$

where $E_{\rm kin}[\rho]$ denotes the kinetic energy, and $E_{\rm xc}[\rho]$ is the unknown exchange and correlation term which contains the energy of the electron-electron interaction except for the Hartree term. Hence all the difficulties of the many-body problem have been transferred into $E_{\rm xc}[\rho]$. Instead of minimizing $E[\rho]$ with respect to ρ one minimizes it w.r.t. a set of one-particle wave functions φ_i related to ρ via

$$\rho(\mathbf{r}) = \sum_{i=1}^{N}|\varphi_i(\mathbf{r})|^2. \tag{5}$$

To guarantee the normalization of φ_i, the Lagrange parameters ε_i are introduced such that the variation $\delta\{E[\rho] + \varepsilon_i[1 - \int d^3r|\varphi_i(\mathbf{r})|^2]\}/\delta\varphi_i(\mathbf{r}) = 0$ yields the Kohn-Sham[2] equations:

$$\left[-\frac{\hbar^2}{2m_e}\Delta + V_{\rm ion}(\mathbf{r}) + \int d^3r'\; V_{\rm ee}(\mathbf{r}-\mathbf{r'})\rho(\mathbf{r'}) + \frac{\delta E_{\rm xc}[\rho]}{\delta\rho(\mathbf{r})}\right]\varphi_i(\mathbf{r}) = \varepsilon_i\;\varphi_i(\mathbf{r}). \tag{6}$$

These equations have the same form as a one-particle Schrödinger equation and yield a kinetic energy for the one-particle wave-function ansatz, i.e., $E_{\rm kin}[\rho_{\rm min}] = -\sum_{i=1}^{N}\langle\varphi_i|\hbar^2\Delta/(2m_e)|\varphi_i\rangle$ where φ_i denote the self-consistent (spin-degenerate) solutions of Eqs. (6) and (5) with lowest "energy" ϵ_i. However, this kinetic energy functional gives not the true kinetic energy of the

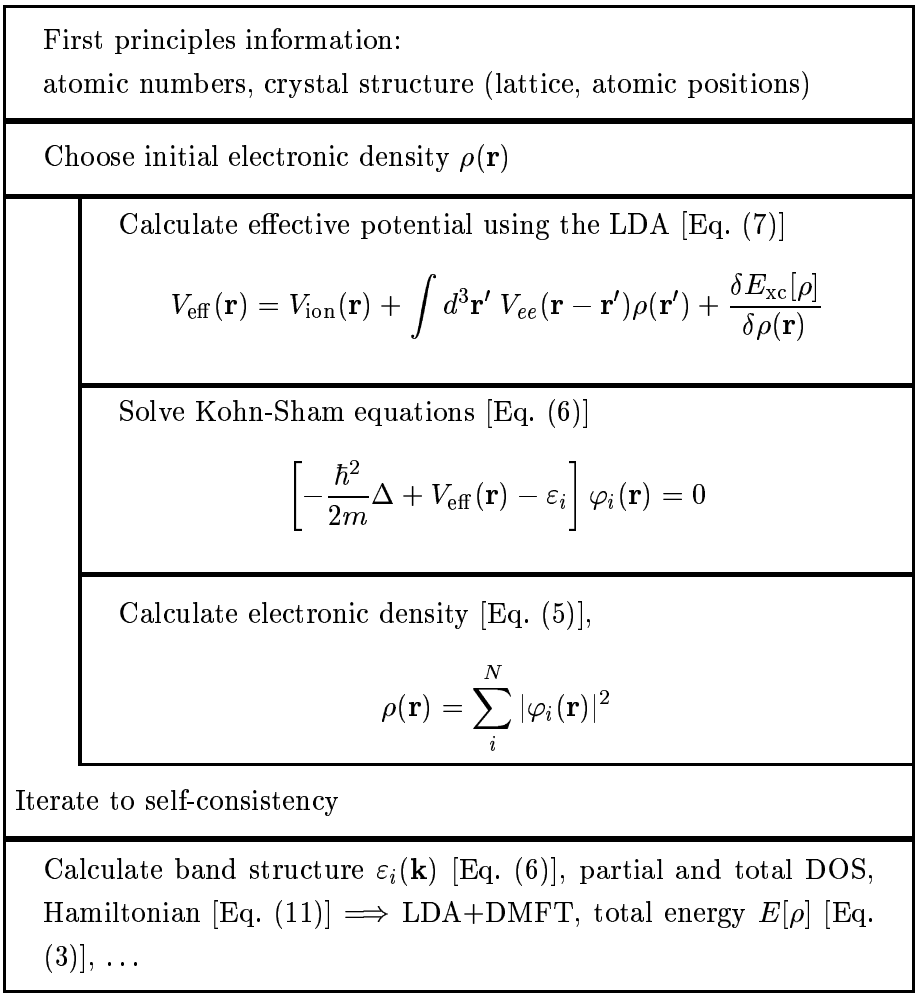

Figure 2: Flow diagram of the DFT/LDA calculations.

correlated problem which would require that the exact $\delta E_{\rm xc}$ also comprises the difference. Also note, that the one-particle potential of Eq. (6), i.e.,

$$V_{\rm eff}(\mathbf{r}) = V_{\rm ion}(\mathbf{r}) + \int d^3r'\, V_{\rm ee}(\mathbf{r}-\mathbf{r}')\rho(\mathbf{r}') + \frac{\delta E_{\rm xc}[\rho]}{\delta\rho(\mathbf{r})}, \tag{7}$$

is only an auxiliary potential which artificially arises in the approach to minimize $E[\rho]$. Thus, the wave functions φ_i and the Lagrange parameters ε_i have no physical meaning at this point. Altogether, these equations allow for the DFT/LDA calculation, see the flow diagram Fig. 2.

2.3 Local density approximation

So far no approximations have been employed since the difficulty of the many-body problem was only transferred to the unknown functional $E_{\rm xc}[\rho]$. For this term the local density approximation (LDA) which approximates the functional $E_{\rm xc}[\rho]$ by a function that depends on the local density only, i.e.,

$$E_{\rm xc}[\rho] \to \int d^3r\, E_{\rm xc}^{\rm LDA}(\rho(\mathbf{r})), \tag{8}$$

was found to be unexpectedly successful. Here, $E_{\rm xc}^{\rm LDA}(\rho(\mathbf{r}))$ is usually calculated from the perturbative solution[10] or the numerical simulation[11] of the jellium problem which is defined by

$V_{\rm ion}(\mathbf{r}) = \text{const.}$

In principle, DFT/LDA only allows one to calculate static properties like the ground state energy or its derivatives. However, one of the major applications of LDA is the calculation of band structures. To this end, the Lagrange parameters ε_i *are interpreted* as the physical (one-particle) energies of the system under consideration. Since the true ground-state is not a simple one-particle wave-function, this is an approximation beyond DFT. Actually, this approximation corresponds to the replacement of the Hamiltonian (1) by

$$\hat{H}_{\rm LDA} = \sum_\sigma \int d^3r\ \hat{\Psi}^+(\mathbf{r},\sigma) \left[\frac{-\hbar^2}{2m_e}\Delta + V_{\rm ion}(\mathbf{r}) + \int d^3r'\, V_{\rm ee}(\mathbf{r}-\mathbf{r}')\rho(\mathbf{r}') + \frac{\delta E_{\rm xc}^{\rm LDA}[\rho]}{\delta\rho(\mathbf{r})} \right] \hat{\Psi}(\mathbf{r},\sigma). \quad (9)$$

For practical calculations one needs to expand the field operators w.r.t. a basis Φ_{ilm}, e.g., a linearized muffin-tin orbital (LMTO)[12,13] basis (i denotes lattice sites; l and m are orbital indices). In this basis,

$$\hat{\Psi}^+(\mathbf{r},\sigma) \quad = \quad \sum_{ilm} \hat{c}_{ilm}^{\sigma\dagger} \Phi_{ilm}(\mathbf{r}) \quad (10)$$

such that the Hamiltonian (9) reads

$$\hat{H}_{\rm LDA} \quad = \quad \sum_{ilm,jl'm',\sigma} (\delta_{ilm,jl'm'}\ \varepsilon_{ilm}\ \hat{n}_{ilm}^\sigma + t_{ilm,jl'm'}\ \hat{c}_{ilm}^{\sigma\dagger}\hat{c}_{jl'm'}^{\sigma}). \quad (11)$$

Here, $\hat{n}_{ilm}^\sigma = \hat{c}_{ilm}^{\sigma\dagger}\hat{c}_{ilm}^{\sigma}$,

$$t_{ilm,jl'm'} = \left\langle \Phi_{ilm} \right| -\frac{\hbar^2\Delta}{2m_e} + V_{\rm ion}(\mathbf{r}) + \int d^3r' V_{\rm ee}(\mathbf{r}-\mathbf{r}')\rho(\mathbf{r}') + \frac{\delta E_{\rm xc}^{\rm LDA}[\rho]}{\delta\rho(\mathbf{r})} \left| \Phi_{jl'm'} \right\rangle \quad (12)$$

for $ilm \neq jl'm'$ and zero otherwise; ε_{ilm} denotes the corresponding diagonal part.

As for static properties, the LDA approach based on the self-consistent solution of Hamiltonian (11) together with the calculation of the electronic density Eq. (5) [see the flow diagram Fig. 2] has also been highly successful for band structure calculations – but only for weakly correlated materials.[3] It is not reliable when applied to correlated materials and can even be completely wrong because it treats electronic *correlations* only very rudimentarily.

2.4 Supplementing LDA with local Coulomb correlations

Of prime importance for correlated materials are the local Coulomb interactions between d- and f-electrons on the same lattice site since these contributions are largest. This is due to the extensive overlap (w.r.t. the Coulomb interaction) of these localized orbitals which results in strong correlations. Moreover, the largest non-local contribution is the nearest-neighbor density-density interaction which, to leading order in the number of nearest-neighbor sites, yields only the Hartree term (see Ref. 14 and, also, Ref. 15) which is already included in the LDA. To take the local Coulomb interactions into account, one can supplement the LDA Hamiltonian (11) with the local Coulomb matrix approximated by the (most important) matrix elements $U_{mm'}^{\sigma\sigma'}$ (Coulomb repulsion and Z-component of Hund's rule coupling) and $J_{mm'}$ (spin-flip terms of Hund's rule coupling) between the localized electrons (for which we assume $i = i_d$ and $l = l_d$):

$$\hat{H} \quad = \quad \hat{H}_{\rm LDA} + \frac{1}{2} \sum_{i=i_d, l=l_d} {\sum_{m\sigma,m'\sigma'}}' U_{mm'}^{\sigma\sigma'} \hat{n}_{ilm\sigma}\hat{n}_{ilm'\sigma'}$$

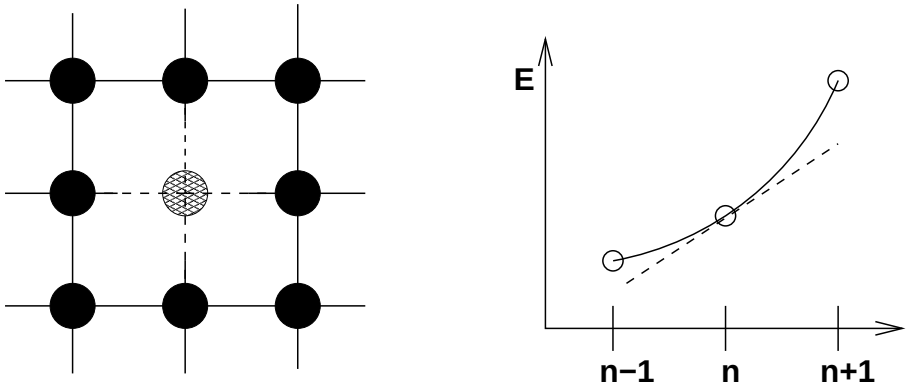

Figure 3: Left: In the constrained LDA calculation the interacting d- or f-electrons on one lattice site are kinetically decoupled from the rest of the system, i.e., they cannot hop to other lattice sites or to other orbitals. By contrast, the *non*-interacting electrons can still still hop to other sites (indicated by dashed lines). Right: This allows one to constrain the number n of interacting d- or f-electrons on the decoupled site and to calculate the corresponding LDA energies $E(n)$ (circles); the dashed line sketches the behavior of $\hat{H}_{\rm LDA}$ defined in Eq. (11).

$$-\frac{1}{2}\sum_{i=i_d,l=l_d}\sum_{m\sigma,m'}{}' J_{mm'}\hat{c}^\dagger_{ilm\sigma}\hat{c}^\dagger_{ilm'\bar{\sigma}}\hat{c}_{ilm'\sigma}\hat{c}_{ilm\bar{\sigma}} - \sum_{i=i_d,l=l_d}\sum_{m\sigma}\Delta\epsilon_d\,\hat{n}_{ilm\sigma}. \qquad (13)$$

Here, the prime on the sum indicates that at least two of the indices of an operator have to be different, and $\bar{\sigma}=\downarrow(\uparrow)$ for $\sigma=\uparrow(\downarrow)$. In principle, also a pair hopping term of the form $\frac{1}{2}\sum_{i=i_d,l=l_d}\sum'_{m\sigma,m'} J_{mm'}\hat{c}^\dagger_{ilm\sigma}\hat{c}^\dagger_{ilm\bar{\sigma}}\hat{c}_{ilm'\sigma}\hat{c}_{ilm'\bar{\sigma}}$ would occur in Eq. (13). This term has not yet been included in LDA+DMFT calculations because one commonly assumes that configurations where one orbital is doubly occupied while another is empty are rare if the Hund's exchange and the hopping terms are included. In typical applications we have $U^{\uparrow\downarrow}_{mm}\equiv U$, $J_{mm'}\equiv J$, $U^{\sigma\sigma'}_{mm'}=U-2J-J\delta_{\sigma\sigma'}$ for $m\neq m'$ (here, the first term $2J$ is due to the reduced Coulomb repulsion between different orbitals and the second term $J\delta_{\sigma\sigma'}$ directly arises from the Z-component of Hund's rule coupling). With the number of interacting orbitals M, the average Coulomb interaction is then

$$\bar{U}=\frac{U+(M-1)(U-2J)+(M-1)(U-3J)}{2M-1}. \qquad (14)$$

The last term of the Hamiltonian (13) reflects a shift of the one-particle potential of the interacting orbitals and is necessary if the Coulomb interaction is taken into account. This last term led to some criticism and we would, thus, like to discuss the origin of this term in more detail below.

The calculation of the local Coulomb interaction $\bar{U}$, or similarly the Hund's exchange constant J, is not at all trivial and requires additional approximations. Presently, the best method available which takes into account screening effects is the constrained LDA method.[16] The basic idea of constrained LDA is to perform LDA calculations for a slightly modified problem, i.e., a problem where the interacting d- or f-electrons of one site are kinetically decoupled from the rest of the system, i.e., their hopping matrix elements $t_{il_dm,jlm'}$ are set to zero, see Fig. 3. This allows one to change the number of interacting electrons on this site. At the same time screening effects of the other electrons, which are redistributed if the number of d- or f-electrons

is changed on the decoupled site, are taken into account. In a LDA+DMFT calculation, one expects an average number n_d of interacting electrons per site on average; typically n_d is close to an integer number. Then, one can do constrained LDA calculations for $n-1$, n, and $n+1$ electrons on the decoupled site, leading to three corresponding total energies, see Fig. 3. The LDA Hamiltonian $\hat{H}_{\rm LDA}$ which was calculated at a fixed density $\rho(r)$ would predict a linear change of the LDA energy with the number of interacting electrons, i.e., $E(n_d) = E_0 + \epsilon_d^{\rm LDA}\, n_d$ with $\epsilon_d^{\rm LDA} = dE^{\rm LDA}/dn_d$. This does not take into account the Coulomb interaction $\bar{U}$ which requires a higher energy cost to add the $(n+1)$th electron than to add the nth electron. This effect leads to the curvature in Fig. 3 and is taken into account in the Hamiltonian (13) which yields $E(n) = E_0 + (1/2)\,\bar{U} n_d(n_d-1) + (\epsilon_d^{\rm LDA} + \Delta\epsilon_d) n_d$. Note, that part of $\Delta\epsilon_d$ just arises to cancel the Coulomb contribution $(1/2)\, d[\bar{U} n_d(n_d-1)]/dn_d = \bar{U}(n_d - 1/2)$. We can, therefore, determine $\bar{U}$ and $\Delta\epsilon_d$ by fitting these parameters to reproduce the constrained LDA energies. That is, we require that Hamiltonian (13) correctly reproduces the LDA energy for three different numbers of interacting electrons on the decoupled site. Similarly, the Hund's exchange J can be calculated by constrained LDA calculations with the spin polarization. One should keep in mind that, while the total LDA spectrum is rather insensitive to the choice of the basis, the constrained LDA calculations of U strongly depends on the shape of the orbitals which are considered to be interacting. E.g., for $LaTiO_3$ at a Wigner Seitz radius of 2.37 a.u. for Ti a LMTO-ASA calculation[17] using the TB-LMTO-ASA code[12] yielded $\bar{U} = 4.2$ eV in comparison to the value $\bar{U} = 3.2$ eV calculated by ASA-LMTO within orthogonal representation.[18] Thus, an appropriate basis is mandatory and, even so, a significant uncertainty in U remains.

In the following, it is convenient to work in reciprocal space where the matrix elements of $\hat{H}^0_{\rm LDA}$, i.e., the LDA one-particle energies without the local Coulomb interaction, are given by

$$(H^0_{\rm LDA}(\mathbf{k}))_{qlm,q'l'm'} = (H_{\rm LDA}(\mathbf{k}))_{qlm,q'l'm'} - \delta_{qlm,q'l'm'}\delta_{ql,q_dl_d}\Delta\epsilon_d\hat{n}_d. \tag{15}$$

Here, q is an index of the atom in the primitive cell, $(H_{\rm LDA}(\mathbf{k}))_{qlm,q'l'm'}$ is the matrix element of (11) in k-space, and q_d denotes the atoms with interacting orbitals in the primitive cell. The non-interacting part, $\hat{H}^0_{\rm LDA}$, supplemented with the local Coulomb interaction forms the (approximated) *ab initio* Hamiltonian for a particular material under investigation:

$$\begin{aligned}\hat{H} &= \hat{H}^0_{\rm LDA} + \frac{1}{2}\sum_{i=i_d,l=l_d}\sum_{m\sigma,m'\sigma'}{}' U^{\sigma\sigma'}_{mm'}\hat{n}_{ilm\sigma}\hat{n}_{ilm'\sigma'} \\ &\quad -\frac{1}{2}\sum_{i=i_d,l=l_d}\sum_{m\sigma,m'}{}' J_{mm'}\hat{c}^\dagger_{ilm\sigma}\hat{c}^\dagger_{ilm'\bar{\sigma}}\hat{c}_{ilm'\sigma}\hat{c}_{ilm\bar{\sigma}}.\end{aligned} \tag{16}$$

2.5 Dynamical mean-field theory

The many-body extension of LDA, Eq. (16), was proposed by Anisimov *et al.*[19] in the context of their LDA+U approach. Within LDA+U the Coulomb interactions of (16) are treated within the Hartree-Fock approximation. Hence, LDA+U does not contain true many-body physics. While this approach is successful in describing long-range ordered, insulating states of correlated electronic systems it fails to describe strongly correlated *paramagnetic* states. To go beyond LDA+U and capture the many-body nature of the electron-electron interaction, i.e., the frequency dependence of the self energy, various approximation schemes have been proposed and

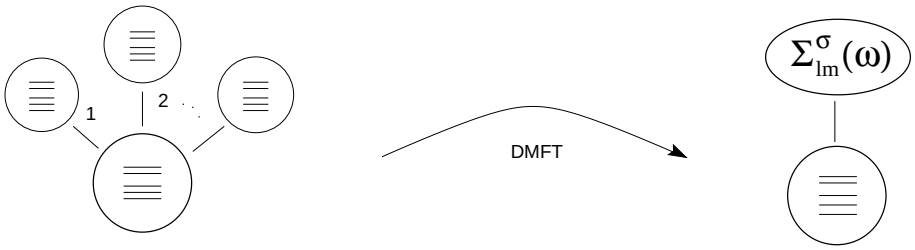

Figure 4: If the number of neighboring lattice sites goes to infinity, the central limit theorem holds and fluctuations from site-to-site can be neglected. This means that the influence of these neighboring sites can be replaced by a mean influence, the dynamical mean-field described by the self energy $\Sigma^{\sigma}_{lm}(\omega)$. This DMFT problem is equivalent to the self-consistent solution of the k-integrated Dyson equation (19) and the multi-band Anderson impurity model Eq. (18). Similar in nature are the coherent potential approximation (CPA) for disorder and the Weiss mean-field theory for spin systems. Indeed, DMFT reduces to these approximations if there is disorder and no Coulomb interaction or if the electrons can be described effectively as localized spins, respectively.

applied recently.[20–25] One of the most promising approaches, first implemented by Anisimov et al.,[20] is to solve (16) within DMFT[14,26–33] ("LDA+DMFT"). Of all extensions of LDA only the LDA+DMFT approach is presently able to describe the physics of *strongly* correlated, paramagnetic metals with well-developed upper and lower Hubbard bands and a narrow quasiparticle peak at the Fermi level. This characteristic three-peak structure is a signature of the importance of many-body effects.[29,30]

During the last ten years, DMFT has proved to be a successful approach for investigating strongly correlated systems with local Coulomb interactions.[33] It becomes exact in the limit of high lattice coordination numbers or dimension d, i.e., it is controlled in $1/d$,[14,26] and preserves the dynamics of local interactions. Hence, it represents a *dynamical* mean-field approximation. In this non-perturbative approach the lattice problem is mapped onto an effective single-site problem (see Fig. 4) which has to be determined self-consistently together with the k-integrated Dyson equation connecting the self energy Σ and the on-site (or in cell) Green function G at frequency ω:

$$G_{qlm,q'l'm'}(\omega) = \frac{1}{V_B}\int d^3k \quad \Big(\big[\, \omega 1 + \mu 1 - H^0_{\rm LDA}(\mathbf{k}) - \Sigma(\omega) \big]^{-1} \Big)_{qlm,q'l'm'} . \tag{17}$$

Here, 1 is the unit matrix, μ the chemical potential, the matrix $H^0_{\rm LDA}(\mathbf{k})$ is defined in (15), $\Sigma(\omega)$ denotes the self energy matrix which is non-zero only between the interacting orbitals, $[...]^{-1}$ implies the inversion of the matrix with elements n $(=qlm)$, $n'(=q'l'm')$, and the integration extends over the Brillouin zone with volume V_B.

The DMFT single-site problem depends on (the Weiss field) $\mathcal{G}(\omega)^{-1} = G(\omega)^{-1} + \Sigma(\omega)$ and is equivalent[29,30] to an Anderson impurity model (the history and the physics of this model is summarized by Anderson in Ref. 34) if its hybridization $\Delta(\omega)$ satisfies $\mathcal{G}^{-1}(\omega) = \omega - \int d\omega' \Delta(\omega')/(\omega - \omega')$. The local one-particle Green function at a Matsubara frequency $i\omega_\nu = i(2\nu+1)\pi/\beta$ (β: inverse temperature), orbital index m $(l = l_d,\ q = q_d)$, and spin σ is given by the following functional integral over Grassmann variables ψ and ψ^* (for an introduction to anti-commuting

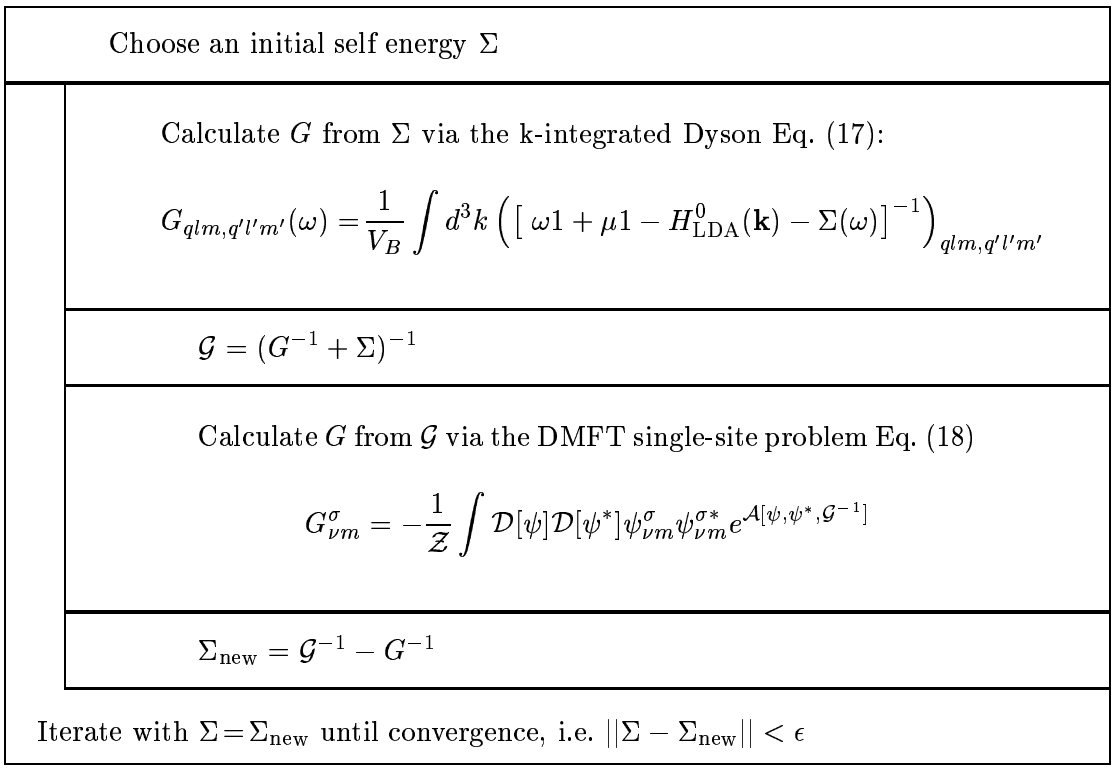

Figure 5: Flow diagram of the DMFT self-consistency cycle.

Grassmann variables see Ref. 35):

$$G^\sigma_{\nu m} = -\frac{1}{\mathcal{Z}}\int \mathcal{D}[\psi]\mathcal{D}[\psi^*]\psi^\sigma_{\nu m}\psi^{\sigma *}_{\nu m} e^{\mathcal{A}[\psi,\psi^*,\mathcal{G}^{-1}]}. \tag{18}$$

Here, $\mathcal{Z} = \int \mathcal{D}[\psi]\mathcal{D}[\psi^*]\psi^\sigma_{\nu m}\psi^{\sigma *}_{\nu m} \exp(\mathcal{A}[\psi,\psi^*,\mathcal{G}^{-1}])$ is the partition function and the single-site action $\mathcal{A}$ has the form (the interaction part of $\mathcal{A}$ is in terms of the "imaginary time" τ, i.e., the Fourier transform of ω_ν)

$$\begin{aligned}\mathcal{A}[\psi,\psi^*,\mathcal{G}^{-1}] = & \sum_{\nu,\sigma,m} \psi^{\sigma *}_{\nu m}(\mathcal{G}^\sigma_{\nu m})^{-1}\psi^\sigma_{\nu m} \\ & -\frac{1}{2}{\sum_{m\sigma,m\sigma'}}' U^{\sigma\sigma'}_{mm'}\int_0^\beta d\tau\, \psi^{\sigma *}_m(\tau)\psi^\sigma_m(\tau)\psi^{\sigma' *}_{m'}(\tau)\psi^{\sigma'}_{m'}(\tau) \\ & +\frac{1}{2}{\sum_{m\sigma,m}}' J_{mm'}\int_0^\beta d\tau\, \psi^{\sigma *}_m(\tau)\psi^{\bar\sigma}_m(\tau)\psi^{\bar\sigma *}_{m'}(\tau)\psi^\sigma_{m'}(\tau)\ .\end{aligned} \tag{19}$$

This single-site problem (18) has to be solved self-consistently together with the **k**-integrated Dyson equation (17) to obtain the DMFT solution of a given problem, see the flow diagram Fig. 5.

Due to the equivalence of the DMFT single-site problem and the Anderson impurity problem a variety of approximate techniques have been employed to solve the DMFT equations, such as the iterated perturbation theory (IPT)[29,33] and the non-crossing approximation (NCA),[36–38] as well as numerical techniques like quantum Monte Carlo simulations (QMC),[39–42] exact diagonalization (ED),[33,43] or numerical renormalization group (NRG).[44] QMC and NCA will be discussed

in more detail in Section 2.6 and 2.7, respectively. IPT is non-self-consistent second-order perturbation theory in U for the Anderson impurity problem (18) at half filling. It represents an ansatz that also yields the correct perturbational U^2-term and the correct atomic limit for the self energy off half filling,[45] for further details see Refs. 20, 21, 45. ED directly diagonalizes the Anderson impurity problem at a limited number of lattice sites and orbitals. NRG first replaces the conduction band by a discrete set of states at $D\Lambda^{-n}$ (D: bandwidth; $n = 0, ..., \mathcal{N}_s$) and then diagonalizes this problem iteratively with increasing accuracy at low energies, i.e., with increasing $\mathcal{N}_s$. In principle, QMC and ED are exact methods, but they require an extrapolation, i.e., the discretization of the imaginary time $\Delta\tau \to 0$ (QMC) or the number of lattice sites of the respective impurity model $N_s \to \infty$ (ED), respectively.

In the context of LDA+DMFT we refer to the computational schemes to solve the DMFT equations discussed above as LDA+DMFT(X) where X=IPT,[20] NCA,[25] QMC[17] have been investigated in the case of $La_{1-x}Sr_xTiO_3$. The same strategy was formulated by Lichtenstein and Katsnelson[21] as one of their LDA++ approaches. Lichtenstein and Katsnelson applied LDA+DMFT(IPT),[46] and were the first to use LDA+DMFT(QMC),[47] to investigate the spectral properties of iron. Recently, among others V_2O_3,[48,49] Ca(Sr)VO_3,[50] LiV_2O_4,[51] $Ca_{2-x}Sr_xRuO_4$,[52,53] CrO_2,[54] Ni,[55] Fe,[55] Mn,[56] Pu,[57,58] and Ce[59–61] have been studied by LDA+DMFT. Realistic investigations of itinerant ferromagnets (e.g., Ni) have also recently become possible by combining density functional theory with multi-band Gutzwiller wave functions.[62]

2.6 QMC method to solve DMFT

The self-consistency cycle of the DMFT (Fig. 5) requires a method to solve for the dynamics of the single-site problem of DMFT, i.e., Eq. (18). The QMC algorithm by Hirsch and Fye[39] is a well established method to find a numerically exact solution for the Anderson impurity model and allows one to calculate the impurity Green function G at a given $\mathcal{G}^{-1}$ as well as correlation functions. In essence, the QMC technique maps the interacting electron problem Eq. (18) onto a sum of non-interacting problems where the single particle moves in a fluctuating, time-dependent field and evaluates this sum by Monte Carlo sampling, see the flow diagram Fig. 6 for an overview. To this end, the imaginary time interval $[0, \beta]$ of the functional integral Eq. (18) is discretized into Λ steps of size $\Delta\tau = \beta/\Lambda$, yielding support points $\tau_l = l\Delta\tau$ with $l = 1 \ldots \Lambda$. Using this Trotter discretization, the integral $\int_0^\beta d\tau$ is transformed to the sum $\sum_{l=1}^{\Lambda} \Delta\tau$ and the exponential terms in Eq. (18) can be separated via the Trotter-Suzuki formula for operators $\hat{A}$ and $\hat{B}$[63]

$$e^{-\beta(\hat{A}+\hat{B})} = \prod_{l=1}^{\Lambda} e^{-\Delta\tau\hat{A}} e^{-\Delta\tau\hat{B}} + \mathcal{O}(\Delta\tau), \tag{20}$$

which is exact in the limit $\Delta\tau \to 0$. The single site action $\mathcal{A}$ of Eq. (19) can now be written in the discrete, imaginary time as

$$\mathcal{A}[\psi, \psi^*, \mathcal{G}^{-1}] = \Delta\tau^2 \sum_{\sigma\, m\, l,l'=0}^{\Lambda-1} \psi^{\sigma}_{ml}{}^* \mathcal{G}^{\sigma\,-1}_m(l\Delta\tau - l'\Delta\tau)\psi^{\sigma}_{ml'}$$

$$-\frac{1}{2}\Delta\tau{\sum_{m\sigma,m'\sigma'}}' U^{\sigma\sigma'}_{mm'} \sum_{l=0}^{\Lambda-1} {\psi^{\sigma}_{ml}}^* \psi^{\sigma}_{ml} {\psi^{\sigma'}_{m'l}}^* \psi^{\sigma'}_{m'l}, \tag{21}$$

where the first term was Fourier-transformed from Matsubara frequencies to imaginary time. In a second step, the $M(2M-1)$ interaction terms in the single site action $\mathcal{A}$ are decoupled by introducing a classical auxiliary field $s^{\sigma\sigma'}_{lmm'}$:

$$\exp\left\{\frac{\Delta\tau}{2} U^{\sigma\sigma'}_{mm'} ({\psi^{\sigma}_{ml}}^* \psi^{\sigma}_{ml} - {\psi^{\sigma'}_{m'l}}^* \psi^{\sigma'}_{m'l})^2\right\} =$$
$$\frac{1}{2} \sum_{s^{\sigma\sigma'}_{lmm'}=\pm 1} \exp\left\{\Delta\tau \lambda^{\sigma\sigma'}_{lmm'} s^{\sigma\sigma'}_{lmm'} ({\psi^{\sigma}_{ml}}^* \psi^{\sigma}_{ml} - {\psi^{\sigma'}_{m'l}}^* \psi^{\sigma'}_{m'l})\right\}, \tag{22}$$

where $\cosh(\lambda^{\sigma\sigma'}_{lmm'}) = \exp(\Delta\tau U^{\sigma\sigma'}_{mm'}/2)$ and M is the number of interacting orbitals. This so-called discrete Hirsch-Fye-Hubbard-Stratonovich transformation can be applied to the Coulomb repulsion as well as the Z-component of Hund's rule coupling.[64] It replaces the interacting system by a sum of $\Lambda M(2M-1)$ auxiliary fields $s^{\sigma\sigma'}_{lmm'}$. The functional integral can now be solved by a simple Gauss integration because the Fermion operators only enter quadratically, i.e., for a given configuration $\mathbf{s} = \{s^{\sigma\sigma'}_{lmm'}\}$ of the auxiliary fields the system is non-interacting. The quantum mechanical problem is then reduced to a matrix problem

$$G^{\tilde{\sigma}}_{\tilde{m}l_1l_2} = \frac{1}{\mathcal{Z}}\frac{1}{2} \sum_{l} {\sum_{m'\sigma',m''\sigma''}}' \sum_{s^{\sigma''\sigma'}_{lm''m'}=\pm 1} \left[(M^{\tilde{\sigma}\mathbf{s}}_{\tilde{m}})^{-1}\right]_{l_1l_2} \prod_{m\sigma} \det \mathbf{M}^{\sigma\mathbf{s}}_{m} \tag{23}$$

with the partition function $\mathcal{Z}$, the matrix

$$\mathbf{M}^{\tilde{\sigma}\mathbf{s}}_{\tilde{m}} = \Delta\tau^2 [{\mathbf{G}^{\sigma}_{m}}^{-1} + \Sigma^{\sigma}_{m}] e^{-\tilde{\lambda}^{\sigma\mathbf{s}}_{m}} + \mathbf{1} - e^{-\tilde{\lambda}^{\sigma\mathbf{s}}_{m}} \tag{24}$$

and the elements of the matrix $\tilde{\lambda}^{\sigma\mathbf{s}}_{m}$

$$\tilde{\lambda}^{\sigma\mathbf{s}}_{mll'} = -\delta_{ll'} \sum_{m'\sigma'} \lambda^{\sigma\sigma'}_{mm'} \tilde{\sigma}^{\sigma\sigma'}_{mm'} s^{\sigma\sigma'}_{lmm'}. \tag{25}$$

Here $\tilde{\sigma}^{\sigma\sigma'}_{mm'} = 2\Theta(\sigma' - \sigma + \delta_{\sigma\sigma'}[m'-m] - 1)$ changes sign if $(m\sigma)$ and $(m'\sigma')$ are exchanged. For more details, e.g., for a derivation of Eq. (24) for the matrix $\mathbf{M}$, see Refs. 33, 39.

Since the sum in Eq. (23) consists of $2^{\Lambda M(2M-1)}$ addends, a complete summation for large Λ is computationally impossible. Therefore the Monte Carlo method, which is often an efficient way to calculate high-dimensional sums and integrals, is employed for importance sampling of Eq. (23). In this method, the integrand $F(x)$ is split up into a normalized probability distribution P and the remaining term O:

$$\int dx F(x) = \int dx\, O(x)\, P(x) \equiv \langle O \rangle_P \tag{26}$$

with

$$\int dx P(x) = 1 \qquad \text{and} \qquad P(x) \geq 0. \tag{27}$$

In statistical physics, the Boltzmann distribution is often a good choice for the function P:

$$P(x) = \frac{1}{\mathcal{Z}} \exp(-\beta E(x)). \tag{28}$$

Choose random auxiliary field configuration $\mathbf{s} = \{s^{\sigma\sigma'}_{lmm'}\}$

Calculate the current Green function $\mathbf{G}_{\rm cur}$ from Eq. (30)

$$(G_{\rm cur})^{\tilde{\sigma}}_{\tilde{m}l_1l_2} = \left[(M^{\tilde{\sigma}\mathbf{s}}_{\tilde{m}})^{-1}\right]_{l_1l_2}$$

with $\mathbf{M}$ from Eq. (24) and the input $\mathcal{G}^{\sigma}_{m}(\omega_\nu)^{-1} = G^{\sigma}_{m}(\omega_\nu)^{-1} + \Sigma^{\sigma}_{m}(\omega_\nu)$.

Do NWU times (warm up sweeps)

- *MC-sweep* $(\mathbf{G}_{\rm cur}, \mathbf{s})$

Do NMC times (measurement sweeps)

- *MC-sweep* $(\mathbf{G}_{\rm cur}, \mathbf{s})$
- $\mathbf{G} = \mathbf{G} + \mathbf{G}_{\rm cur}/\mathrm{NMC}$

Figure 6: Flow diagram of the QMC algorithm to calculate the Green function matrix $\mathbf{G}$ using the procedure *MC-sweep* of Fig. 7.

For the sum of Eq. (23), this probability distribution translates to

$$P(\mathbf{s}) = \frac{1}{\mathcal{Z}} \prod_{m\sigma} \det \mathbf{M}^{\sigma\mathbf{s}}_{m} \tag{29}$$

with the remaining term

$$O(\mathbf{s})^{\tilde{\sigma}}_{\tilde{m}l_1l_2} = \left[(M^{\tilde{\sigma}\mathbf{s}}_{\tilde{m}})^{-1}\right]_{l_1l_2}. \tag{30}$$

Instead of summing over all possible configurations, the Monte Carlo simulation generates configurations x_i according to the probability distribution $P(x)$ and averages the observable $O(x)$ over these x_i. Therefore the relevant parts of the phase space with a large Boltzmann weight are taken into account to a greater extent than the ones with a small weight, coining the name importance sampling for this method. With the central limit theorem one gets for $\mathcal{N}$ statistically independent addends the estimate

$$\langle O\rangle_P = \frac{1}{\mathcal{N}} \sum_{x_i\in P(x) i=1}^{\mathcal{N}} O(x_i) \pm \frac{1}{\sqrt{\mathcal{N}}} \sqrt{\langle O^2\rangle_P - \langle O\rangle_P^2}. \tag{31}$$

Here, the error and with it the number of needed addends $\mathcal{N}$ is nearly independent of the dimension of the integral. The computational effort for the Monte Carlo method is therefore only rising polynomially with the dimension of the integral and not exponentially as in a normal integration. Using a Markov process and single spin-flips in the auxiliary fields, the computational cost of the algorithm in leading order of Λ is

$$2aM(2M-1)\Lambda^3 \times \text{number of MC-sweeps}, \tag{32}$$

where a is the acceptance rate for a single spin-flip.

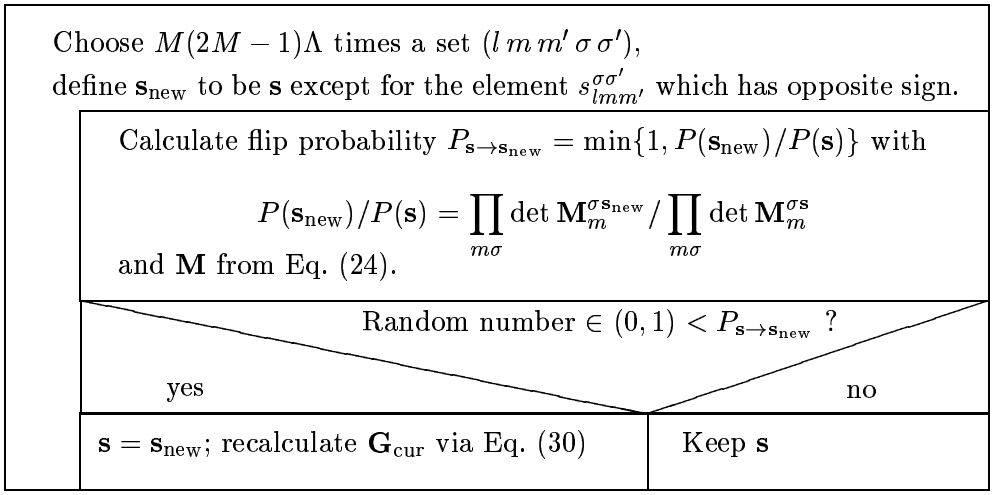

Figure 7: Procedure *MC-sweep* using the Metropolis[65] rule to change the sign of $s^{\sigma\sigma'}_{lmm'}$. The recalculation of $\mathbf{G}_{\rm cur}$, i.e., the matrix $\mathbf{M}$ of Eq. (24), simplifies to $\mathcal{O}(\Lambda^2)$ operations if only one $s^{\sigma\sigma'}_{lmm'}$ changes sign.[33, 39]

The advantage of the QMC method (for the algorithm see the flow diagram Fig. 6) is that it is (numerically) exact. It allows one to calculate the one-particle Green function as well as two-particle (or higher) Green functions. On present workstations the QMC approach is able to deal with up to seven *interacting* orbitals and temperatures above about room temperature. Very low temperatures are not accessible because the numerical effort grows like $\Lambda^3 \propto 1/T^3$. Since the QMC approach calculates $G(\tau)$ or $G(i\omega_n)$ with a statistical error, it also requires the maximum entropy method[66] to obtain the Green function $G(\omega)$ at real (physical) frequencies ω.

2.7 NCA method to solve DMFT

The NCA approach is a resolvent perturbation theory in the hybridization parameter $\Delta(\omega)$ of the effective Anderson impurity problem.[36] Thus, it is reliable if the Coulomb interaction U is large compared to the band-width and also offers a computationally inexpensive approach to check the general spectral features in other situations.

To see how the NCA can be adapted for the DMFT, let us rewrite Eq. (17) as

$$G_\sigma(z) = \frac{1}{N_k} \sum_{\mathbf{k}} \left[z - H^0_{LDA}(\mathbf{k}) - \Sigma_\sigma(z) \right]^{-1} \tag{33}$$

where $z = \omega + i0^+ + \mu$. Again, $H^0_{LDA}(\mathbf{k})$, $\Sigma_\sigma(z)$ and, hence, $G^0_\sigma(\zeta)$ and $G_\sigma(z)$ are matrices in orbital space. Note that $\Sigma(z)$ has nonzero entries for the correlated orbitals only.

On quite general grounds, Eq. (33) can be cast into the form

$$G_\sigma(z) = \frac{1}{z - E^0 - \Sigma_\sigma(z) - \Delta_\sigma(z)} \tag{34}$$

where

$$E^0 = \frac{1}{N_k} \sum_{\mathbf{k}} H^0_{LDA}(\mathbf{k}) \tag{35}$$

with the number of k points N_k and

$$\lim_{\omega\to\pm\infty} \Re e\{\Delta_\sigma(\omega+i\delta)\} = 0 \ . \tag{36}$$

Given the matrix E^0, the Coulomb matrix U and the hybridization matrix $\Delta_\sigma(z)$, we are now in a position to set up a resolvent perturbation theory with respect to $\Delta_\sigma(z)$. To this end, we first have to diagonalize the local Hamiltonian

$$\begin{aligned} H_{\rm local} = & \sum_\sigma \sum_{qml} \sum_{q'm'l'} c^\dagger_{qlm\sigma} E^0_{qlm,q'l'm'} c_{qlm\sigma} + \frac{1}{2}\sum_{m\sigma}\sum_{m'\sigma'} U^{\sigma\sigma'}_{mm'} n_{q_d l_d m\sigma} n_{q_d l_d m'\sigma'} \\ & -\frac{1}{2}\sum_{m\sigma}\sum_{m'} J_{mm'} c^\dagger_{q_d l_d m\sigma} c^\dagger_{q_d l_d m'\bar\sigma} c_{q_d l_d m'\sigma} c_{q_d l_d m\bar\sigma} \\ = & \sum_\alpha E_\alpha |\alpha\rangle\langle\alpha| \end{aligned} \tag{37}$$

with local eigenstates $|\alpha\rangle$ and energies E_α. In contrast to the QMC, this approach allows one to take into account the full Coulomb matrix plus spin-orbit coupling.

With the states $|\alpha\rangle$ defined above, the fermionic operators with quantum numbers $\kappa = (q,l,m)$ are expressed as

$$\begin{aligned} c^\dagger_{\kappa\sigma} &= \sum_{\alpha,\beta} \left(D^{\kappa\sigma}_{\beta\alpha}\right)^* |\alpha\rangle\langle\beta| \ , \\ c_{\kappa\sigma} &= \sum_{\alpha,\beta} D^{\kappa\sigma}_{\alpha\beta} |\alpha\rangle\langle\beta| \ . \end{aligned} \tag{38}$$

The key quantity for the resolvent perturbation theory is the resolvent $R(z)$, which obeys a Dyson equation[36]

$$R(z) = R^0(z) + R^0(z) S(z) R(z) \ , \tag{39}$$

where $R^0_{\alpha\beta}(z) = 1/(z-E_\alpha)\delta_{\alpha\beta}$ and $S_{\alpha\beta}(z)$ denotes the self energy for the local states due to the coupling to the environment through $\Delta(z)$.

The self energy $S_{\alpha\beta}(z)$ can be expressed as power series in the hybridization $\Delta(z)$.[36] Retaining only the lowest-, i.e. 2^{nd}-order terms leads to a set of self-consistent integral equations

$$\begin{aligned} S_{\alpha\beta}(z) = & \sum_\sigma \sum_{\kappa\kappa'} \sum_{\alpha'\beta'} \int \frac{d\varepsilon}{\pi} f(\varepsilon)\ (D^{\kappa\sigma}_{\alpha'\alpha})^*\, \Gamma^{\kappa\kappa'}_\sigma(\varepsilon) R_{\alpha'\beta'}(z+\varepsilon) D^{\kappa'\sigma}_{\beta'\beta} \\ & + \sum_\sigma \sum_{\kappa\kappa'} \sum_{\alpha'\beta'} \int \frac{d\varepsilon}{\pi} \left(1-f(\varepsilon)\right) D^{\kappa\sigma}_{\alpha'\alpha} \Gamma^{\kappa\kappa'}_\sigma(\varepsilon) R_{\alpha'\beta'}(z-\varepsilon) \left(D^{\kappa'\sigma}_{\beta'\beta}\right)^* \end{aligned} \tag{40}$$

to determine $S_{\alpha\beta}(z)$, where $f(\varepsilon)$ denotes Fermi's function and $\Gamma(\varepsilon) = -\Im m\left\{\Delta(\varepsilon+i0^+)\right\}$. The set of equations (40) is in the literature referred to as non-crossing approximation (NCA), because, when viewed in terms of diagrams, these diagrams contain no crossing of band-electron lines. In order to close the cycle for the DMFT, we still have to calculate the true local Green function $G_\sigma(z)$. This, however, can be done within the same approximation with the result

$$G^{\kappa\kappa'}_\sigma(i\omega) = \frac{1}{Z_{\rm local}} \sum_{\alpha,\alpha'} \sum_{\nu,\nu'} D^{\kappa\sigma}_{\alpha\alpha'} \left(D^{\kappa'\sigma}_{\nu\nu'}\right)^* \oint \frac{dz e^{-\beta z}}{2\pi i} R_{\alpha\nu}(z) R_{\alpha'\nu'}(z+i\omega) \ . \tag{41}$$

Here, $Z_{\rm local} = \sum_\alpha \oint \frac{dz e^{-\beta z}}{2\pi i} R_{\alpha\alpha}(z)$ denotes the local partition function and β is the inverse temperature.

Like any other technique, the NCA has its merits and disadvantages. As a self-consistent resummation of diagrams it constitutes a conserving approximation to the Anderson impurity model. Furthermore, it is a (computationally) fast method to obtain dynamical results for this model and thus also within DMFT. However, the NCA is known to violate Fermi liquid properties at temperatures much lower than the smallest energy scale of the problem and whenever charge excitations become dominant.[38,67] Hence, in some parameter ranges it fails in the most dramatic way and must therefore be applied with considerable care.[38]

2.8 Simplifications for transition metal oxides with well separated e_g- and t_{2g}-bands

Many transition metal oxides are cubic perovskites, with only a slight distortion of the cubic crystal structure. In these systems the transition metal d-orbitals lead to strong Coulomb interactions between the electrons. The cubic crystal-field of the oxygen causes the d-orbitals to split into three degenerate t_{2g}- and two degenerate e_g-orbitals. This splitting is often so strong that the t_{2g}- or e_g-bands at the Fermi energy are rather well separated from all other bands. In this situation the low-energy physics is well described by taking only the degenerate bands at the Fermi energy into account. Without symmetry breaking, the Green function and the self energy of these bands remain degenerate, i.e., $G_{qlm,q'l'm'}(z) = G(z)\delta_{qlm,q'l'm'}$ and $\Sigma_{qlm,q'l'm'}(z) = \Sigma(z)\delta_{qlm,q'l'm'}$ for $l = l_d$ and $q = q_d$ (where l_d and q_d denote the electrons in the interacting band at the Fermi energy). Downfolding to a basis with these degenerate q_d-l_d-bands results in an effective Hamiltonian $H^{0\,\rm eff}_{\rm LDA}$ (where indices $l = l_d$ and $q = q_d$ are suppressed)

$$G_{mm'}(\omega) \;=\; \frac{1}{V_B}\int \mathrm{d}^3k\, \left([\omega 1 + \mu 1 - H^{0\,\rm eff}_{\rm LDA}(\mathbf{k}) - \Sigma(\omega)]^{-1} \right)_{mm'} . \tag{42}$$

Due to the diagonal structure of the self energy the degenerate interacting Green function can be expressed via the non-interacting Green function $G^0(\omega)$:

$$G(\omega) \;=\; G^0(\omega - \Sigma(\omega)) = \int d\epsilon \frac{N^0(\epsilon)}{\omega - \Sigma(\omega) - \epsilon}. \tag{43}$$

Thus, it is possible to use the Hilbert transformation of the unperturbed LDA-calculated density of states (DOS) $N^0(\epsilon)$, i.e., Eq. (43), instead of Eq. (17). This simplifies the calculations considerably. With Eq. (43) also some conceptual simplifications arise: (i) the subtraction of $\sum_{i=i_d,l=l_d}\sum_{m\sigma}\Delta\epsilon_d\,\hat{n}_{ilm\sigma}$ [see Eq. (13)] only results in an (unimportant) shift of the chemical potential in (43) and, thus, the exact form of $\Delta\epsilon_d$ is irrelevant; (ii) Luttinger's theorem of Fermi pinning holds, i.e., the interacting DOS at the Fermi energy is fixed at the value of the non-interacting DOS at $T = 0$ within a Fermi liquid; (iii) as the number of electrons within the different bands is fixed, the LDA+DMFT approach is automatically self-consistent.

3 Extensions and modifications of LDA+DMFT

3.1 Self-consistent LDA+DMFT calculations

In the present form of the LDA+DMFT scheme the band-structure input due to LDA and the inclusion of the electronic correlations by DMFT are performed as successive steps without subsequent feedback. In general, the DMFT solution will result in a change of the occupation of the different bands involved. This changes the electron density $\rho(\mathbf{r})$ and, thus, results in a new LDA-Hamiltonian $\hat{H}_{\mathrm{LDA}}$ (11) since $\hat{H}_{\mathrm{LDA}}$ depends on $\rho(\mathbf{r})$. At the same time also the Coulomb interaction U changes and needs to be determined by a new constrained LDA calculation. In a *self-consistent* LDA+DMFT scheme, H_{LDA} and U would define a new Hamiltonian (16) which again needs to be solved within DMFT, etc., until convergence is reached:

$$\rho(\mathbf{r}) \longrightarrow H_{\mathrm{LDA}},\, U \xrightarrow{\text{DMFT}} n_{ilm} \longrightarrow \rho(\mathbf{r}) \tag{44}$$

Without Coulomb interaction ($U = 0$) this scheme reduces to the self-consistent solution of the Kohn-Sham equations. A self-consistency scheme similar to Eq. (44) was employed by Savrasov and Kotliar[58] in their calculation of Pu (without self-consistency for U). The quantitative difference between non-self-consistent and self-consistent LDA+DMFT depends on the change of the number of electrons in the different bands after the DMFT calculation, which of course depends on the problem at hand. E.g., for the Ce calculation presented in Section 6, this change was very minor in the vicinity of α-γ transition but more significant at lower volumes.

In this context, we would also like to note that an *ab initio* DMFT scheme formulated directly in the continuum was recently proposed by Chitra and Kotliar.[68]

3.2 LDA+DMFT as a spectral density functional theory

Our derivation of the LDA+DMFT method was physically motivated. That is, we started from the assumption that the Kohn-Sham equations, i.e., the LDA part, yield the correct results for the weakly correlated s- or p-bands, while the DMFT-part takes into account the local Coulomb interactions of the strongly correlated d- or f-bands. Using the effective action construction by Fukuda *et al.*,[69] Savrasov *et al.*[7,57,58] embedded LDA+DMFT in a functional theory with a functional $E[G_{il_dm}(\omega), \rho(r)]$ which depends on the electron density $\rho(r)$ *and* the local Green function $G_{il_dm}(\omega)$ (thus coining the name *spectral density functional theory*[7]). This is in the spirit of density functional theory with the LDA+DMFT equations emerging from the minimization of $E[G_{il_dm}(\omega), \rho(r)]$ w.r.t. $G_{il_dm}(\omega)$ and $\rho(r)$. If the functional $E[G_{il_dm}(\omega), \rho(r)]$ were known exactly one would obtain the exact ground state energy. However, since the exact functional is unknown one has to introduce approximations. Then, LDA+DMFT is a workable approximation to the spectral density function theory, similar to LDA within DFT.

3.3 Cluster extensions of DMFT

DMFT reliably describes local correlations in terms of the local (or, equivalently k-independent) self energy $\Sigma_{il_dm,il_dm'}(\omega)$. For some problems like, e.g., fluctuations in the vicinity of a phase transition or the formation of a spin-singlet on two neighboring sites, non-local correlations are important. The standard DMFT described in Section 2.5 neglects such non-local correlations because only a single site with local correlations in an average environment (a dynamical mean-field) is considered. However, in principle, DMFT can also treat more than one site, i.e., a cell of sites, in an average environment. E.g., if the primitive contains several sites with interacting d- or f-orbitals a natural choice for the DMFT cell would be this cell. Then, non-local correlations $\Sigma_{il_dm,jl_dm'}(\omega)$ would be taken into account if i and j are within the cell, whereas such correlations would be neglected if i and j are located in different cells. Furthermore, even if the primitive contains only one interacting site one may consider a larger DMFT cell with several interacting sites, treating non-local correlations within that cell but not between different cells. This is the basic idea of cluster DMFT approaches.[33,70–72]

An alternative scheme, named dynamical cluster approximation (DCA), has been proposed by Hettler *et al.*[73] The DCA has the advantage of preserving the translational symmetry. While cluster DMFT can be best understood in real space, it is instructive to go to k-space for DCA. Within DCA the first Brillouin zone is divided into N_c patches around k-vectors K, assuming the self energy to be constant within each patch only (in contrast to DMFT, where the self energy is constant for all k-vectors). In real space, the DCA cluster has periodic boundary conditions instead of open boundary conditions for the cluster DMFT scheme. In addition, the dynamical mean-field couples to every site of the cluster, whereas within cluster DMFT it couples exclusively to the boundary sites. Whether cluster DMFT or DCA provides a better scaling w.r.t. cluster size $N_c \to \infty$ is still a matter of debate and likely depends on the problem at hand (both approaches give the correct behavior of any finite-dimensional problem for $N_c \to \infty$). It is important to note, and not a matter of course, that all these approaches[70–73] lead to physically correct (causal) Green functions.

A third route was proposed by Schiller *et al.*[74] It is a natural extension of DMFT in the sense that it takes into account all diagrams to next order in $1/d$ (d: spatial dimension), i.e., up to order $1/d$. This leads to a theory with a single-site and a two-site cluster whose Green functions have to be subtracted.

Cluster extensions of DMFT have been applied successfully to a couple of model systems. For example, d-wave superconductivity in the two-dimensional Hubbard model mediated by spin-fluctuations was found.[71,75] In the context of LDA+DMFT cluster extensions of DMFT are still work in progress.

3.4 GW+DMFT

A possible alternative to LDA+DMFT is the GW+DMFT[77] approach, which uses Hedin's GW approximation[76] instead of the LDA to generate the multi-band many-body problem Eq. (16) in Section 2.4. From a pure, theoretical point of view, GW+DMFT has the advantage of being a fully diagrammatic approach. This allows a better understanding of what one is actually

calculating and is particularly appealing to the many-body community. One might consider GW+DMFT as the minimum set of diagrams which are necessary to realistically describe correlated materials: It contains the Hartree and exchange diagrams together with the RPA-like screening of the Coulomb interaction and, via DMFT, the important local diagrams leading to the Kondo-like and Mott-insulating physics of correlated systems. However, whether these theoretical principles can be maintained in actual calculations still needs to be seen. Problems already arise in mere GW calculations of weakly correlated systems where Coulomb interactions are (often) calculated from the (non-diagrammatic) LDA wave function instead of the self-consistent GW wave functions. GW+DMFT calculations for real materials are still work in progress.[77]

4 Comparison of different methods to solve DMFT: the model system $La_{1-x}Sr_xTiO_3$

The stoichiometric compound $LaTiO_3$ is a cubic perovskite with a small orthorhombic distortion ($\angle\, Ti-O-Ti \approx 155°$)[78] and is an antiferromagnetic insulator[79] below $T_N = 125$ K.[80] Above T_N, or at low Sr-doping x, and neglecting the small orthorhombic distortion (i.e., considering a cubic structure with the same volume), $LaTiO_3$ is a strongly correlated, but otherwise simple paramagnet with only *one* $3d$-electron on the trivalent Ti sites. This makes the system a perfect trial candidate for the LDA+DMFT approach.

The LDA band-structure calculation for undoped (cubic) $LaTiO_3$ yields the DOS shown in Fig. 8 which is typical for early transition metal oxides. The oxygen bands, ranging from -8.2 eV to -4.0 eV, are filled such that Ti has a d^1 configuration. Due to the crystal- or ligand-field splitting, the Ti $3d$-bands separate into two empty e_g-bands and three degenerate t_{2g}-bands. Since the t_{2g}-bands at the Fermi energy are well separated also from the other bands we employ the approximation introduced in section 2.5 which allows us to work with the LDA DOS [Eq. (43)] instead of the full one-particle Hamiltonian $H^0_{\rm LDA}$ of [Eq. (17)]. In the LDA+DMFT calculation, Sr-doping x is taken into account by adjusting the chemical potential to yield $n = 1 - x = 0.94$ electrons within the t_{2g}-bands, neglecting effects of disorder and the x-dependence of the LDA DOS (note, that $LaTiO_3$ and $SrTiO_3$ have a very similar band structure within LDA). There is some uncertainty in the LDA-calculated Coulomb interaction parameter $U \sim 4-5$ eV (for a discussion see Ref. 17) which is here assumed to be spin- and orbital-independent. In Fig. 9, results for the spectrum of $La_{0.94}Sr_{0.06}TiO_3$ as calculated by LDA+DMFT(IPT, NCA, QMC) for the same LDA DOS at $T \approx 1000$ K and $U = 4$ eV are compared.[17] In Ref. 17 the formerly presented IPT[20] and NCA[25] spectra were recalculated to allow for a comparison at exactly the same parameters. All three methods yield the typical features of strongly correlated metallic paramagnets: a lower Hubbard band, a quasi-particle peak (note that IPT produces a quasi-particle peak only below about 250K which is therefore not seen here), and an upper Hubbard band. By contrast, within LDA the correlation-induced Hubbard bands are missing and only a broad central quasi-particle band (actually a one-particle peak) is obtained (Fig. 8).

While the results of the three evaluation techniques of the DMFT equations (the approximations IPT, NCA and the numerically exact method QMC) agree on a qualitative level, Fig. 9 reveals

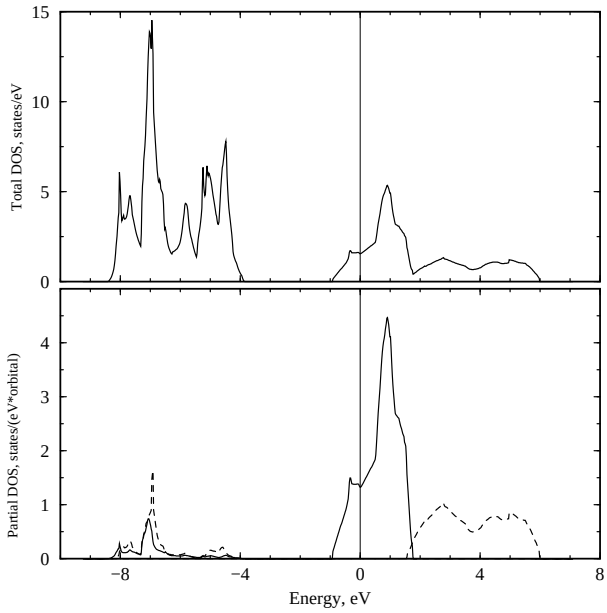

Figure 8: Densities of states of $LaTiO_3$ calculated with LDA-LMTO. Upper figure: total DOS; lower figure: partial t_{2g} (solid lines) and e_g (dashed lines) DOS [reproduced from Ref. 17].

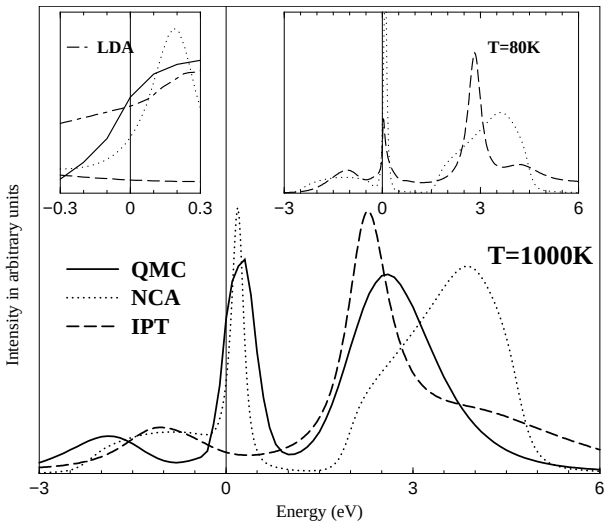

Figure 9: Spectrum of $La_{0.94}Sr_{0.06}TiO_3$ as calculated by LDA+DMFT(X) at $T = 0.1$ eV ($\approx$ 1000 K) and $U = 4$ eV employing the approximations X=IPT, NCA, and numerically exact QMC. Inset left: Behavior at the Fermi level including the LDA DOS. Inset right: X=IPT and NCA spectra at $T = 80$ K [reproduced from Ref. 17].

considerable quantitative differences. In particular, the IPT quasi-particle peak found at low temperatures (see right inset of Fig. 9) is too narrow such that it disappears already at about 250 K and is, thus, not present at $T \approx 1000$ K. A similarly narrow IPT quasi-particle peak was found in a three-band model study with Bethe-DOS by Kajueter and Kotliar.[45] Besides underestimating the Kondo temperature, IPT also produces notable deviations in the shape of the upper Hubbard band. Although NCA comes off much better than IPT it still underestimates the width of the quasiparticle peak by a factor of two. Furthermore, the position of the quasi-particle peak is too close to the lower Hubbard band. In the left inset of Fig. 9, the spectra at the Fermi level are shown. At the Fermi level, where at sufficiently low temperatures the interacting DOS should be pinned at the non-interacting value, the NCA yields a spectral function which is almost by a factor of two too small. The pinning of the interacting DOS mentioned above holds for the situation here where only degenerate bands are involved and the system is a Fermi liquid. It is due to the k-independence of the self-energy; nonetheless, the effective mass is renormalized: $m^*/m_0 = 1 - \partial\Re\Sigma(w)/\partial\omega|_{\omega=0}$. The shortcomings of the NCA-results, with a too small low-energy scale and too much broadened Hubbard bands for multi-band systems, are well understood and related to the neglect of exchange type diagrams.[82] Similarly, the deficiencies of the IPT-results are not entirely surprising in view of the semi-phenomenological nature of this approximation, especially for a system off half filling.

This comparison shows that the choice of the *method* used to solve the DMFT equations is indeed *important*, and that, at least for the present system, the approximations IPT and NCA differ quantitatively from the numerically exact QMC. Nevertheless, the NCA gives a rather good account of the qualitative spectral features and, because it is fast and can often be applied at comparatively low temperatures, can yield an overview of the physics.

Photoemission spectra provide a direct experimental tool to study the electronic structure and spectral properties of electronically correlated materials. A comparison of LDA+DMFT(QMC) at 1000 K[83] with the experimental photoemission spectrum[84] of $La_{0.94}Sr_{0.06}TiO_3$ is presented in Fig 10. To take into account the uncertainty in U,[17] we present results for $U = 3.2$, 4.25 and 5 eV. All spectra are multiplied with the Fermi step function and are Gauss-broadened with a broadening parameter of 0.3 eV to simulate the experimental resolution.[84] LDA band structure calculations, the results of which are also presented in Fig. 10, clearly fail to reproduce the broad band observed in the experiment at 1-2 eV below the Fermi energy.[84] Taking the correlations between the electrons into account, this lower band is easily identified as the lower Hubbard band whose spectral weight originates from the quasi-particle band at the Fermi energy and which increases with U. The best agreement with experiment concerning the relative intensities of the Hubbard band and the quasi-particle peak and, also, the position of the Hubbard band is found for $U = 5$ eV. The value $U = 5$ eV is still compatible with the *ab initio* calculation of this parameter within LDA.[17] One should also bear in mind that photoemission experiments are sensitive to surface properties. Due to the reduced coordination number at the surface the bandwidth is likely to be smaller, and the Coulomb interaction less screened, i.e., larger. Both effects make the system more correlated and, thus, might also explain why better agreement is found for $U = 5$ eV. Besides that, also the polycrystalline nature of the sample, as well as spin and orbital[85] fluctuation not taken into account in the LDA+DMFT approach, will lead to a further reduction of the quasi-particle weight.

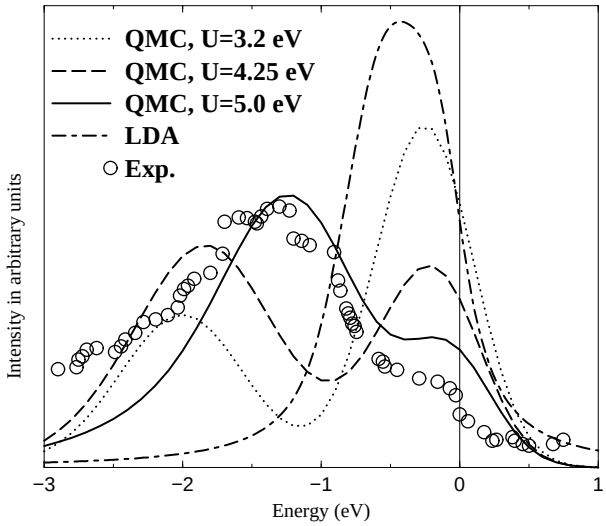

Figure 10: Comparison of the experimental photoemission spectrum,[84] the LDA result, and the LDA+DMFT(QMC) calculation for $La_{0.94}Sr_{0.06}TiO_3$ (i.e., 6% hole doping) and different Coulomb interactions $U = 3.2$, 4.25, and 5 eV [reproduced from Ref.17].

5 Mott-Hubbard metal-insulator transition in V_2O_3

One of the most famous examples of a cooperative electronic phenomenon occurring at intermediate coupling strengths is the transition between a paramagnetic metal and a paramagnetic insulator induced by the Coulomb interaction between the electrons – the Mott-Hubbard metal-insulator transition. The question concerning the nature of this transition poses one of the fundamental theoretical problems in condensed matter physics.[86] Correlation-induced metal-insulator transitions (MIT) are found, for example, in transition metal oxides with partially filled bands near the Fermi level. For such systems bandstructure theory typically predicts metallic behavior. The most famous example is V_2O_3 doped with Cr as shown in Fig. 11. While at low temperatures V_2O_3 is an antiferromagnetic insulator with monoclinic crystal symmetry, it has a corundum structure in the high-temperature paramagnetic phase. All transitions shown in the phase diagram are of first order. In the case of the transitions from the high-temperature paramagnetic phases into the low-temperature antiferromagnetic phase this is naturally explained by the fact that the transition is accompanied by a change in crystal symmetry. By contrast, the crystal symmetry across the MIT in the paramagnetic phase remains intact, since only the ratio of the c/a axes changes discontinuously. This may be taken as an indication for the predominantly electronic origin of this transition which is not accompanied by any conventional long-range order. ¿From a model point of view the MIT is triggered by a change of the ratio of the Coulomb interaction U relative to the bandwidth W. Originally, Mott considered the extreme limits $W = 0$ (when atoms are isolated and insulating) and $U = 0$ where the system is metallic. While it is simple to describe these limits, the crossover between them, i.e., the metal-insulator transition itself, poses a very complicated electronic correlation problem. Among others, this metal-insulator transition has been addressed by Hubbard in various approximations[88] and by Brinkman and Rice within the Gutzwiller approximation.[89] During the last few years, our understanding of the MIT in the one-band Hubbard model has considerably

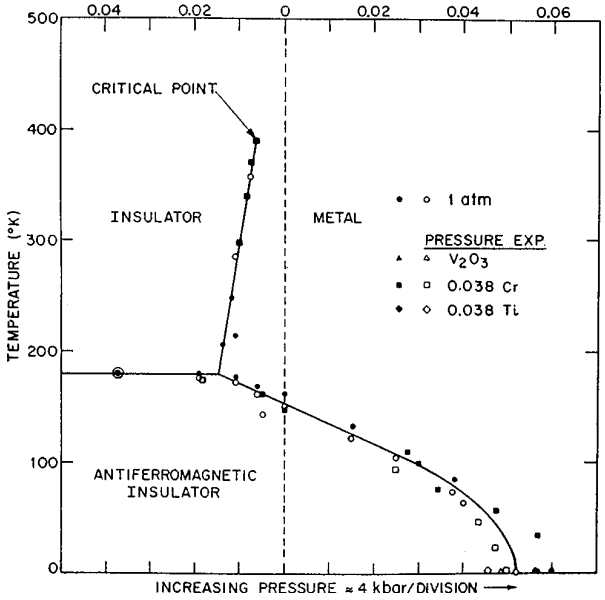

Figure 11: Experimental phase diagram of V_2O_3 doped with Cr and Ti [reproduced from Ref. 87]. Doping V_2O_3 affects the lattice constants in a similar way as applying pressure (generated either by a hydrostatic pressure P, or by changing the V-concentration from V_2O_3 to $V_{2-y}O_3$) and leads to a Mott-Hubbard transition between the *paramagnetic* insulator (PI) and metal (PM). At lower temperatures, a Mott-Heisenberg transition between the paramagnetic metal (PM) and the *antiferromagnetic* insulator (AFI) is observed.

improved, in particular due to the application of dynamical mean-field theory.[90]

Both the paramagnetic *metal* V_2O_3 and the paramagnetic *insulator* $(V_{0.962}Cr_{0.038})_2O_3$ have the same corundum crystal structure with only slightly different lattice parameters.[91,92] Nevertheless, within LDA both phases are found to be metallic (see Fig. 12). The LDA DOS shows a splitting of the five Vanadium d-orbitals into three t_{2g} states near the Fermi energy and two e_g^σ states at higher energies. This reflects the (approximate) octahedral arrangement of oxygen around the vanadium atoms. Due to the trigonal symmetry of the corundum structure the t_{2g} states are further split into one a_{1g} band and two degenerate e_g^π bands, see Fig. 12. The only visible difference between $(V_{0.962}Cr_{0.038})_2O_3$ and V_2O_3 is a slight narrowing of the t_{2g} and e_g^σ bands by ≈ 0.2 and 0.1 eV, respectively as well as a weak downshift of the centers of gravity of both groups of bands for V_2O_3. In particular, the insulating gap of the Cr-doped system is seen to be missing in the LDA DOS. Here we will employ LDA+DMFT(QMC) to show explicitly that the insulating gap is caused by electronic correlations. In particular, we make use of the simplification for transition metal oxides described in Section 2.8 and restrict the LDA+DMFT(QMC) calculation to the three t_{2g} bands at the Fermi energy, separated from the e_g^σ and oxygen bands.

While the Hund's rule coupling J is insensitive to screening effects and may, thus, be obtained within LDA to a good accuracy ($J = 0.93$ eV[18]), the LDA-calculated value of the Coulomb repulsion U has a typical uncertainty of at least 0.5 eV.[17] To overcome this uncertainty, we study the spectra obtained by LDA+DMFT(QMC) for three different values of the Hubbard interaction ($U = 4.5, 5.0, 5.5$ eV) in Fig. 13. ¿From the results obtained we conclude that the critical value of U for the MIT is at about 5 eV: At $U = 4.5$ eV one observes pronounced

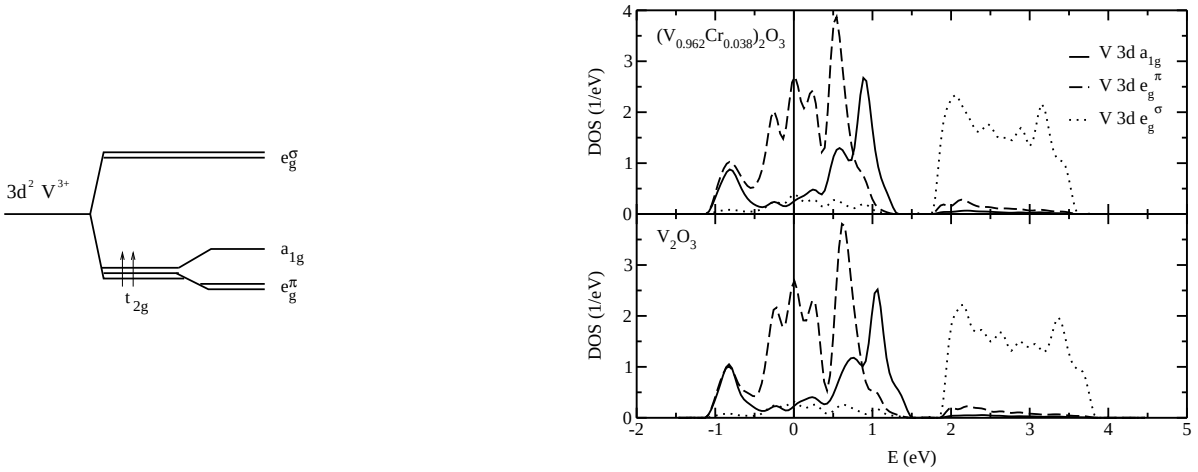

Figure 12: Left: Scheme of the $3d$ levels in the corundum crystal structure. Right: Partial LDA DOS of the 3d bands for paramagnetic metallic V_2O_3 and insulating $(V_{0.962}Cr_{0.038})_2O_3$ [reproduced from Ref. 48].

quasiparticle peaks at the Fermi energy, i.e., characteristic metallic behavior, even for the crystal structure of the insulator $(V_{0.962}Cr_{0.038})_2O_3$, while at $U = 5.5$ eV the form of the calculated spectral function is typical for an insulator for both sets of crystal structure parameters. At $U = 5.0$ eV one is then at, or very close to, the MIT since there is a pronounced dip in the DOS at the Fermi energy for both a_{1g} and e_g^π orbitals for the crystal structure of $(V_{0.962}Cr_{0.038})_2O_3$, while for pure V_2O_3 one still finds quasiparticle peaks. (We note that at $T \approx 0.1$ eV one only observes metallic-like and insulator-like behavior, with a rapid but smooth crossover between these two phases, since a sharp MIT occurs only at lower temperatures[40,90]). The critical value of the Coulomb interaction $U \approx 5$ eV is in reasonable agreement with the values determined spectroscopically by fitting to model calculations, and by constrained LDA, see Ref. 48 for details.

To compare with the V_2O_3 photoemission spectra by Schramme *et al.*[93] and Mo *et al.*,[94] as well as with the X-ray absorption data by Müller *et al.*,[95] the LDA+DMFT(QMC) spectrum at $T = 300$ K is multiplied with the Fermi function and Gauss-broadened by 0.09 eV to account for the experimental resolution. The theoretical result for $U = 5$ eV is seen to be in good agreement with experiment (Fig. 14). In contrast to the LDA results, our results do not only describe the different bandwidths above *and* below the Fermi energy (≈ 6 eV and $\approx 2-3$ eV, respectively), but also the position of two (hardly distinguishable) peaks below the Fermi energy (at about -1 eV and -0.3 eV) as well as the pronounced two-peak structure above the Fermi energy (at about 1 eV and 3-4 eV). In our calculation the e_g^σ states have not been included so far. Taking into account the Coulomb interaction $\bar{U} = U - 2J \approx 3$ eV and also the difference between the e_g^σ- and t_{2g}-band centers of gravity of roughly 2.5 eV, the e_g^σ-band can be expected to be located roughly 5.5 eV above the lower Hubbard band (-1.5 eV), i.e., at about 4 eV. From this estimate one would conclude the upper X-ray absorption maximum around 4 eV in Fig. 12 to be of mixed e_g^σ and e_g^π nature.

While LDA also gives two peaks below and above the Fermi energy, their position and physical origin is quite different. Within LDA+DMFT(QMC) the peaks at -1 eV and 3-4 eV are the incoherent Hubbard bands induced by the electronic correlations whereas in the LDA the peak

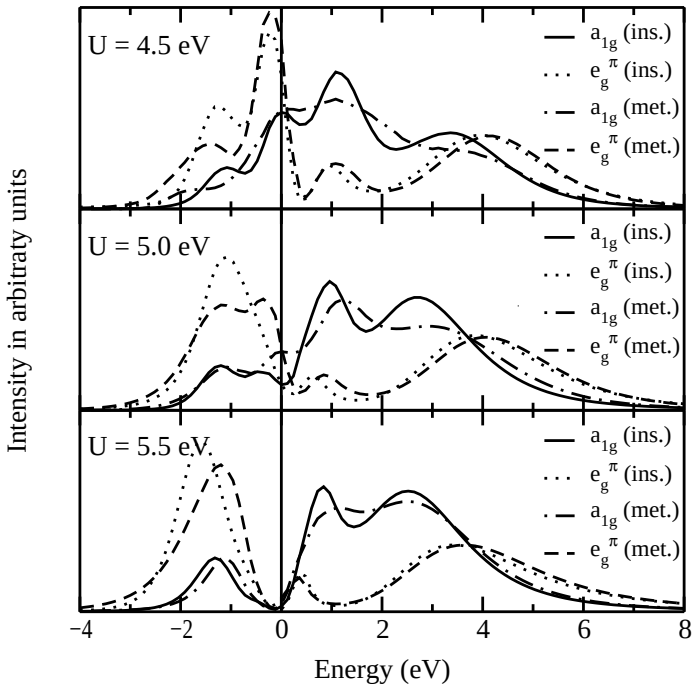

Figure 13: LDA+DMFT(QMC) spectra for paramagnetic $(V_{0.962}Cr_{0.038})_2O_3$ ("ins.") and V_2O_3 ("met.") at $U = 4.5$, 5 and 5.5 eV, and $T = 0.1$ eV $= 1160$ K [reproduced from Ref.48].

at 2-3 eV is caused entirely by (one-particle) e_g^σ states, and that at -1 eV is the band edge maximum of the a_{1g} and e_g^π states (see Fig. 12). Obviously, the LDA+DMFT results are a big improvement over LDA which, as one should keep in mind, was the best method available to calculate the V_2O_3 spectrum before. Still there remain some differences between theory and experiment which might, among other reasons, be due to the fact that every V ion has a unique neighbor in one direction, i.e., the LDA supercell calculation has *a pair* of V ions per primitive cell, or due to short-range antiferromagnetic correlations in the vicinity of the antiferromagnetic transition (175 K is close to the Néel temperature).

Particularly interesting are the spin and the orbital degrees of freedom in V_2O_3. From our calculations,[48] we conclude that the spin state of V_2O_3 is $S = 1$ throughout the Mott-Hubbard transition region. This agrees with the measurements of Park *et al.*[96] and also with the data for the high-temperature susceptibility.[97] But, it is at odds with the $S=1/2$ model by Castellani *et al.*[98] and with the results[99] for a one-band Hubbard model which corresponds to $S=1/2$ in the insulating phase and, contrary to our results, shows a substantial change of the local magnetic moment at the MIT.[90] For the orbital degrees of freedom we find a predominant occupation of the e_g^π orbitals, but with a significant admixture of a_{1g} orbitals. This admixture decreases at the MIT: in the metallic phase at $T = 0.1$ eV we determine the occupation of the (a_{1g}, e_{g1}^π, e_{g2}^π) orbitals as (0.37, 0.815, 0.815), and in the insulating phase as (0.28, 0.86, 0.86). This should be compared with the experimental results of Park *et al.*[96] From their analysis of the linear dichroism data the authors concluded that the ratio of the configurations $e_g^\pi e_g^\pi$:$e_g^\pi a_{1g}$ is equal to 1:1 for the paramagnetic metallic and 3:2 for the paramagnetic insulating phase, corresponding to a one-electron occupation of (0.5,0.75,0.75) and (0.4,0.8,0.8), respectively. Although our results show a somewhat smaller value for the admixture of a_{1g} orbitals, the overall behavior,

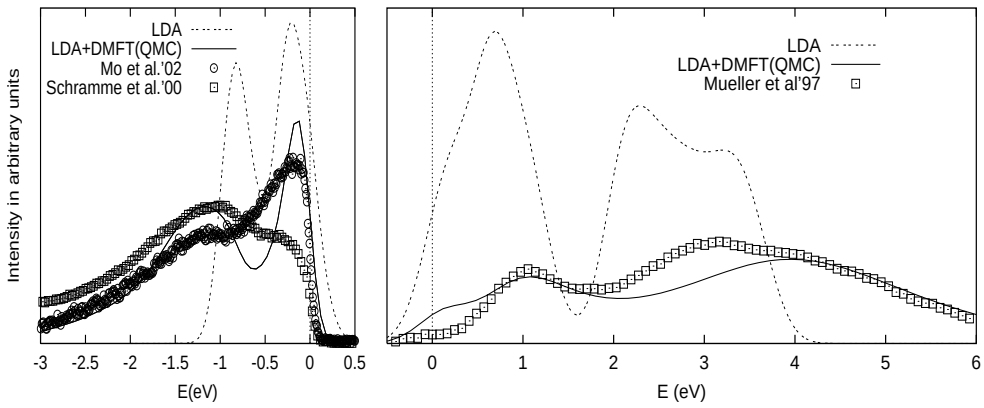

Figure 14: Comparison of the LDA+DMFT(QMC) spectrum[48] at $U = 5\,\mathrm{eV}$ and $T = 300\,\mathrm{K}$ below (left Figure) and above (right Figure) the Fermi energy (at 0 eV) with the LDA spectrum[48] and the experimental spectrum (left: photoemission spectrum of Schramme *et al.*[93] at $T = 300\,\mathrm{K}$ and Mo *et al.* at $T = 175\,\mathrm{K}$;[94] right: X-ray absorption spectrum of Müller *et al.* at $T = 300\,\mathrm{K}$[95]). Note that Mo *et al.*[94] use a higher photon energy ($h\nu = 500\,\mathrm{eV}$) than Schramme *et al.*[93] ($h\nu = 60\,\mathrm{eV}$) which considerably reduces the surface contribution to the spectrum.

including the tendency of a *decrease* of the a_{1g} admixture across the transition to the insulating state, are well reproduced. In this context we would also like to note the work by Laad *et al.*[49] who started from our LDA DOS for V_2O_3 and found, within DMFT(IPT), that it is possible to trigger a Mott-Hubbard metal-insulator transition by shifting the e_g^π-band with respect to the a_{1g}-band.

In the study above, the experimental crystal parameters of V_2O_3 and $(V_{0.962}Cr_{0.038})_2O_3$ have been taken from the experiment. This leaves the question unanswered whether a change of the lattice is the driving force behind the Mott transition, or whether it is the electronic Mott transition which causes a change of the lattice. For another system, Ce, we will show in Section 6 that the energetic changes near a Mott transition are indeed sufficient to cause a first-order volume change.

6 The Cerium volume collapse: An example for a $4f$-electron system

Cerium exhibits a transition from the γ- to the α-phase with increasing pressure or decreasing temperature. This transition is accompanied by an unusually large volume change of 15%,[100] much larger than the 1-2% volume change in V_2O_3. The γ-phase may also be prepared in metastable form at room temperature in which case the γ-α transition occurs under pressure at this temperature.[101] Similar volume collapse transitions are observed under pressure in Pr and Gd (for a recent review, see Ref. 102). It is widely believed that these transitions arise from changes in the degree of $4f$ electron correlations, as is reflected in both the Mott transition[103] and the Kondo volume collapse (KVC)[104] models.

The Mott transition model envisions a change from itinerant, bonding character of the $4f$-

electrons in the α-phase to non-bonding, localized character in the γ-phase, driven by changes in the $4f$-$4f$ inter-site hybridization. Thus, as the ratio of the $4f$ Coulomb interaction to the $4f$-bandwidth increases, a Mott transition occurs to the γ-phase, similar to the Mott-Hubbard transition of the $3d$-electrons in V_2O_3 (Section 5).

The Kondo volume collapse[104] scenario ascribes the collapse to a strong change in the energy scale associated with the screening of the local $4f$-moment by conduction electrons (Kondo screening), which is accompanied by the appearance of an Abrikosov-Suhl-like quasiparticle peak at the Fermi level. In this model the $4f$-electron spectrum of Ce would change across the transition in a fashion very similar to the Mott scenario, i.e., a strong reduction of the spectral weight at the Fermi energy should be observed in going from the α- to the γ-phase. The subtle difference comes about by the γ-phase having metallic f-spectra with a strongly enhanced effective mass as in a heavy fermion system, in contrast to the f-spectra characteristic of an insulator in the case of the Mott scenario. The f-spectra in the Kondo picture also exhibit Hubbard side-bands not only in the γ-phase, but in the α-phase as well, at least close to the transition. While local-density and static mean-field theories correctly yield the Fermi-level peaks in the f-spectra for the α-phase, they do not exhibit such additional Hubbard side-bands, which is sometimes taken as characteristic of the "α-like" phase in the Mott scenario.[103] However, this behavior is more likely a consequence of the static mean-field treatment, as correlated solutions of both Hubbard and periodic Anderson models exhibit such residual Hubbard side-bands in the α-like regimes.[105]

Typically, the Hubbard model and the periodic Anderson model are considered as paradigms for the Mott and KVC model, respectively. Although both models describe completely different physical situations it was shown recently that one can observe a surprisingly similar behavior at finite temperatures: the evolution of the spectrum and the local magnetic moment with increasing Coulomb interaction show very similar features as well as, in the case of a periodic Anderson model with nearest neighbor hybridization, the phase diagram and the charge compressibility.[105,106] From this point of view the distinction between the two scenarios appears to be somewhat artificial, at least at temperatures relevant for the description of the α-γ transition.

For a realistic calculation of the cerium α-γ transition, we employ the full Hamiltonian calculation described in Sections 2.3, 2.4, and 2.5 where the one-particle Hamiltonian was calculated by LDA and the $4f$ Coulomb interaction U along with the associated $4f$ site energy shift by a constrained LDA calculation (for details of the two independent calculations presented in the current Section see Refs. 60, 61, 102 and Ref. 59). We have not included the spin-orbit interaction which has a rather small impact on LDA results for Ce, nor the intra-atomic exchange interaction which is less relevant for Ce as occupations with more than one $4f$-electron on the same site are rare [$J = 0$ in Eq. (13)]. Furthermore, the $6s$-, $6p$-, and $5d$-orbitals are assumed to be non-interacting in the formalism of Eq. (13), Section 2.4. Note, that the $4f$ orbitals are even better localized than the $3d$ orbitals and, thus, uncertainties in U and the 4f site energy [$\Delta\epsilon_d$ in (13)] are relatively small and would only translate into a possible volume shift for the α-γ-transition.

The LDA+DMFT(QMC) spectral evolution of the Ce $4f$-electrons is presented in Fig. 15. It shows similarities to V_2O_3 (Fig. 13, Section 5): At a volume per atom $V = 20\,\text{Å}^3$, Fig. 15 shows

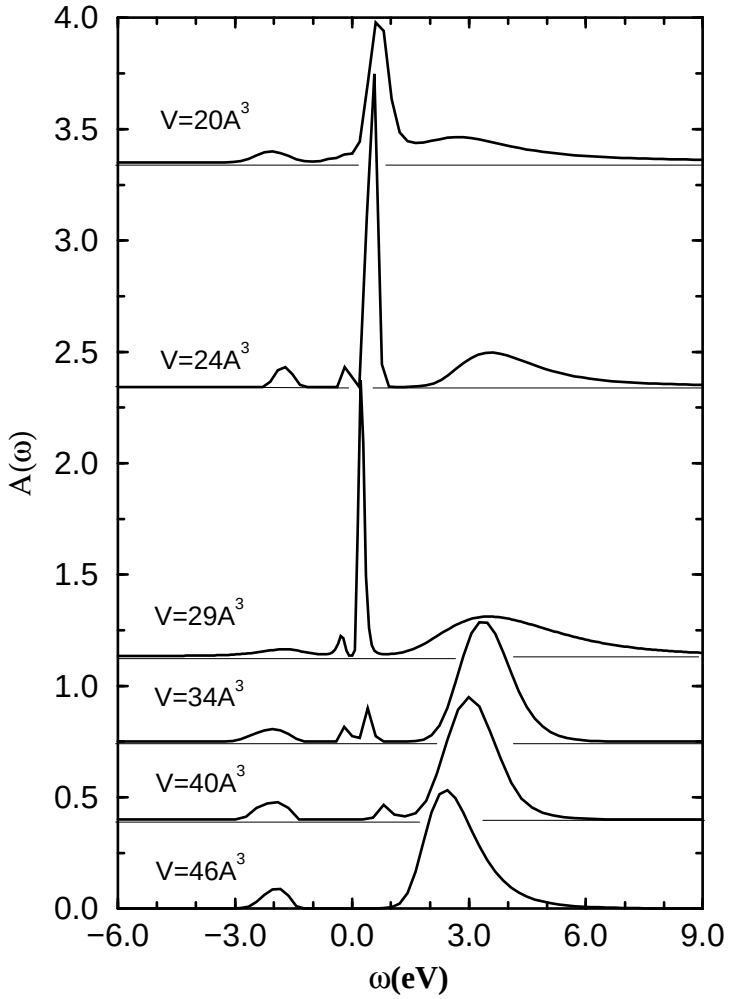

Figure 15: Evolution of the $4f$ spectral function $A(\omega)$ with volume at $T = 632\,\mathrm{K}$ ($\omega = 0$ corresponds to the chemical potential; curves are offset as indicated; $\Delta\tau = 0.11\mathrm{eV}^{-1}$). Coinciding with the sharp anomaly in the correlation energy (Fig. 16), the central quasiparticle resonance disappears, at least at finite temperatures [reproduced from Ref. 61].

that almost the entire spectral weight lies in a large quasiparticle peak with a center of gravity slightly above the chemical potential. This is similar to the LDA solution; however, a weak upper Hubbard band is also present even at this small volume. At the volumes $29\,\text{Å}^3$ and $34\,\text{Å}^3$ which approximately bracket the α-γ transition, the spectrum has a three peak structure. Finally, by $V = 46$ Å^3, the central peak has disappeared leaving only the lower and upper Hubbard bands. However, an important difference to V_2O_3 is that the *spd*-spectrum shows metallic behavior and, thus, cerium remains a metal throughout this transition monitored by a vanishing $4f$ quasiparticle resonance.

To study the energetic changes associated with the rapid change of the quasiparticle weight at the Fermi energy, we calculate the DMFT energy per site for the model Hamiltonian (13)

$$E_{\mathrm{DMFT}} = \frac{T}{N_k} \sum_{n\mathbf{k}\sigma} \mathrm{Tr}(H^0_{\mathrm{LDA}}(\mathbf{k}) G_{\mathbf{k}}(i\omega_n)) e^{i\omega_n 0^+} + U_f\, d. \tag{45}$$

Here, Tr denotes the trace over the 16×16 matrices, T the temperature, N_k the number of k points, $G_{\mathbf{k}}$ the Green function matrix w.r.t. the orbital indices, $H^0_{\mathrm{LDA}}(\mathbf{k})$ the LDA one-particle

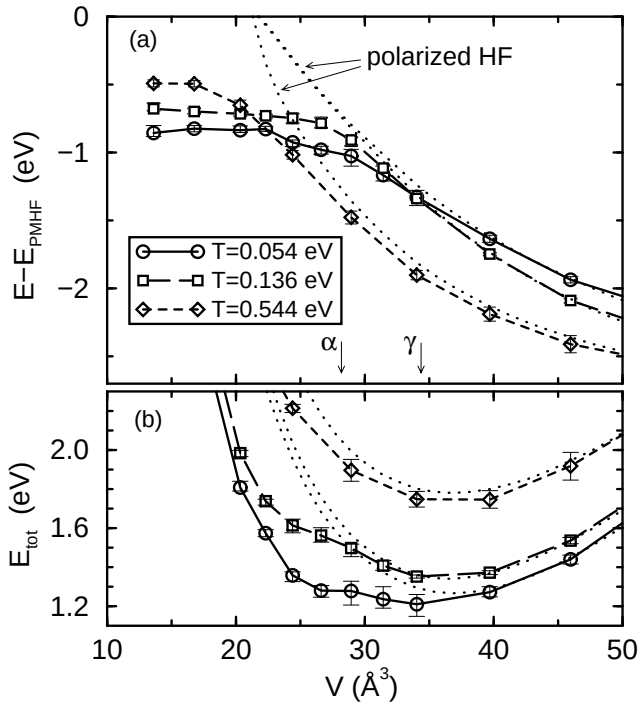

Figure 16: (a) Correlation energy $E_{\rm DMFT} - E_{\rm PMHF}$ as a function of atomic volume (symbols) and polarized HF energy $E_{\rm AFHF} - E_{\rm PMHF}$ (dotted lines which, at large V, approach the DMFT curves for the respective temperatures); arrows: observed volume collapse from the α- to the γ-phase. The correlation energy sharply bends away from the polarized HF energy in the region of the transition. (b) The resultant negative curvature leads to a growing depression of the total energy near $V = 26$–28 Å^3 as temperature is decreased, consistent with an emerging double well at still lower temperatures and thus the α-γ transition. The curves at $T = 0.544$ eV were shifted downwards in (b) by -0.5 eV to match the energy range [reproduced from Ref. 60].

matrix Eq. (15), and

$$d = \frac{1}{2}{\sum}'_{m\sigma,m'\sigma'} \langle \hat{n}_{ifm\sigma}\, \hat{n}_{ifm'\sigma'} \rangle \tag{46}$$

is a generalization of the one-band double occupation for multi-band models.

Fig. 16a shows our calculated DMFT(QMC) energies $E_{\rm DMFT}$ as a function of atomic volume at three temperatures *relative* to the paramagnetic Hartree Fock (HF) energies $E_{\rm PMHF}$ [of the Hamiltonian (13)], i.e., the energy contribution due to *electronic correlations*. We also present the polarized HF energies which basically represent a (non-self-consistent) LDA+U calculation and reproduce $E_{\rm DMFT}$ at large volumes and low temperatures. With decreasing volume, however, the DMFT energies bend away from the polarized HF solutions. Thus, at $T = 0.054\,{\rm eV} \approx 600\,{\rm K}$, a region of negative curvature in $E_{\rm DMFT} - E_{\rm PMHF}$ is evident within the observed two phase region (arrows).

Fig. 16b presents the calculated LDA+DMFT total energy $E_{\rm tot}(T) = E_{\rm LDA}(T) + E_{\rm DMFT}(T) - E_{\rm mLDA}(T)$ where $E_{\rm mLDA}$ is the energy of an LDA-like solution of the Hamiltonian (13).[107] Since both $E_{\rm LDA}$ and $E_{\rm PMHF} - E_{\rm mLDA}$ have positive curvature throughout the volume range considered, it is the negative curvature of the correlation energy in Fig. 16a which leads to the dramatic depression of the LDA+DMFT total energies in the range $V = 26$-28 Å^3 for decreasing

	α-Ce LDA+DMFT(QMC)	α-Ce LDA+DMFT(NCA)	α-Ce exp[108,109]	γ-Ce LDA+DMFT(QMC)	γ-Ce LDA+DMFT(NCA)	γ-Ce exp[108,109]
P_0	0.12 ± 0.03	0.126	0.1558	0.01 ± 0.02	0.0150	0.0426
P_1	0.77 ± 0.03	0.829	0.8079	0.94 ± 0.03	0.9426	0.9444
P_2	0.11 ± 0.01	0.044	0.0264	0.05 ± 0.01	0.0423	0.0131
n_f	0.99 ± 0.01	0.908	$0.8 \ldots 0.861$	1.04 ± 0.02	1.014	$0.971 \ldots 1$
T_K, [K]	≈ 2100	1000	$945 \ldots 2000$	n.a.	30	$60 \ldots 95$
χ, $[10^{-3}\frac{\text{emu}}{\text{mol}}]$	n.a.	1.08	$0.53 \ldots 0.70$	n.a.	24	$8.0 \ldots 12$

Table 1: Comparison between LDA+DMFT(QMC)[61] and LDA+DMFT(NCA)[59] calculated parameters for both α- and γ-phase and experimental values.[108,109] P_0, P_1 and P_2 are partial probabilities for an empty, singly and doubly occupied $4f$-state, n_f is the f-electron occupancy, $T_{\rm K}$ the estimated Kondo temperature, and χ the magnetic susceptibility.

temperature, which contrasts to the smaller changes near $V = 34\,\text{Å}^3$ in Fig. 16b. This trend is consistent with a double well structure emerging at still lower temperatures (prohibitively expensive for QMC simulations), and with it a first-order volume collapse. This is in reasonable agreement with the experimental volume collapse. Further physical quantities like the free energy and the specific heat are presented in Ref. 61. Also note that a similar scenario has been proposed recently for the δ-α transition in Pu on the basis of LDA+DMFT calculations,[57] which solves DMFT by an ansatz inspired by IPT and includes a modification of the DFT/LDA step to account for the density changes introduced by the DMFT.[58]

In the LDA+DMFT(QMC) and in a separate LDA+DMFT(NCA)[59] calculation for Ce, we have obtained a number of physical quantities for both phases which may be compared to experimental values. Various static properties extracted from the calculations and their counterparts extracted from experiments are collected in Table 1 and show an overall fair to good agreement in the tendencies and, except for the susceptibility, the absolute values. The differences between LDA+DMFT(QMC)[61] and LDA+DMFT(NCA)[59] are most likely due to the different method employed to solve the DMFT self-consistency equations. But also, difference in the LDA treatment and, for α-Ce, in the Coulomb interaction U might matter (in Ref. 59, U was assumed to be the same for α- and γ-Ce, whereas the *ab initio* determination of U in Ref. 102 which was employed in Refs. 60, 61 yield a slightly smaller U-value for α- than for γ-Ce). Since the calculation of the magnetic susceptibility χ in Ref. 59 was based on simplifying assumptions, the absolute numbers cannot be expected to match experiment. However, the general tendency and especially the ratio between α- and γ-Ce is in good agreement with experiment. It is interesting to note that the experiments predict a finite Kondo screening-scale for both phases, which actually would point toward the KVC scenario.

Finally, let us compare the spectral functions calculated with the LDA+DMFT(QMC) approach to experimental data.[110] The photoemission spectrum for α-Ce (upper part of Fig. 17) shows a main structure between 3 eV and 7 eV, which is attributed to $4f^2$ final state multiplets. In the calculated spectrum all excitations to $4f^2$ states are described by the featureless upper

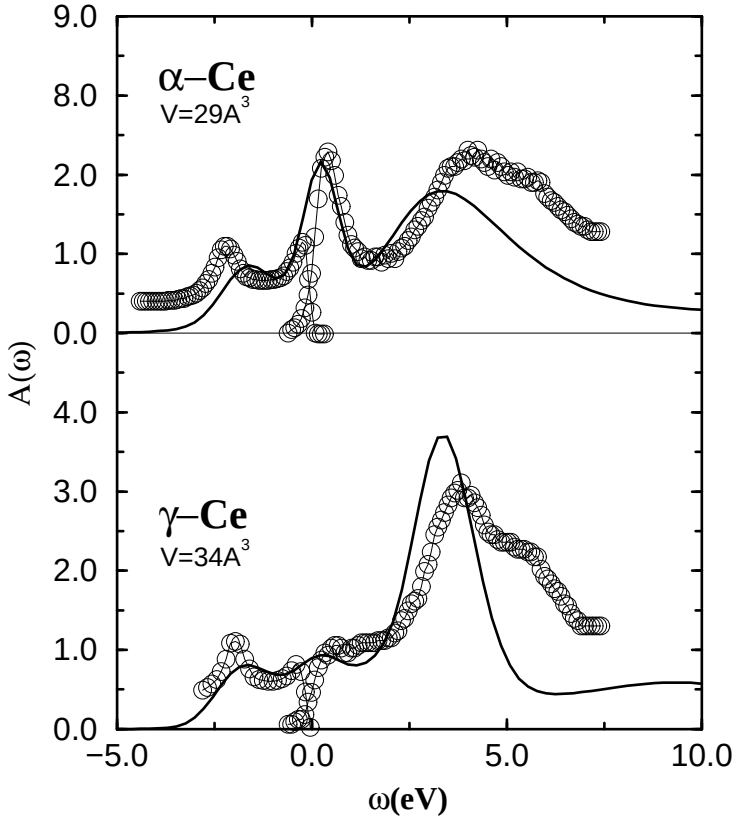

Figure 17: Comparison between combined photoemission[110] and BIS[111] experimental (circles) and theoretical LDA+DMFT(QMC) total spectra (solid line) for α- (upper part) and γ-Ce (lower part) at $T = 580\,\mathrm{K}$. The experimental and theoretical spectra were normalized and the theoretical curve was broadened with resolution width of 0.4 eV [reproduced from Ref. 61].

Hubbard band. As a consequence of the simplified interaction model all doubly occupied states are degenerate. This shortcoming in our calculation is responsible for the sharply peaked main structure. The neglected exchange interaction would produce a multiplet structure, which would be closer to the experiment. The calculated f-spectrum shows a sharp quasiparticle or Kondo resonance slightly above the Fermi energy, which is the result of the formation of a singlet state between f- and conduction states. We thus suggest that the spectral weight seen in the experiment is a result of this quasiparticle resonance. In the lower part of Fig. 17, a comparison between experiment and our calculation for γ-Ce is shown. The most striking difference between the lower and the upper part of Fig. 17 is the absence of the Kondo resonance in the γ-phase which is in agreement with our calculations. Nonetheless γ-Ce remains metallic with spectral weight arising from the *spd*-electrons at the Fermi energy. Altogether, one can say that the agreement with the experimental spectrum is very good, and comparable to the LDA accuracy for much simpler systems.

7 Conclusion and Outlook

At present LDA+DMFT is the only available *ab initio* computational technique which is able to treat correlated electronic systems close to a Mott-Hubbard MIT, heavy fermions, and f-electron materials. The physical properties of such systems are characterized by the correlation-induced

generation of small, Kondo-like energy scales which are missing in the LDA and which require the application of genuine many-body techniques.

In this paper we discussed the set-up of the computational scheme LDA+DMFT which merges two non-perturbative, complementary investigation techniques for many-particle systems in solid state physics. LDA+DMFT allows one to perform *ab initio* calculations of real materials with strongly correlated electrons. Using the band structure results calculated within local density approximation (LDA) as input, the missing electronic correlations are introduced by dynamical mean-field theory (DMFT). On a technical level this requires the solution of an effective self-consistent, multi-band Anderson impurity problem by some numerical method (e.g. IPT, NCA, QMC). Comparison of the photoemission spectrum of $La_{1-x}Sr_xTiO_3$ calculated by LDA+DMFT using IPT, NCA, and QMC reveal that the choice of the evaluation method is of considerable importance. Indeed, only with the numerically exact QMC quantitatively reliable results are obtained. The results of the LDA+DMFT(QMC) approach were found to be in good agreement with the experimental photoemission spectrum of $La_{0.94}Sr_{0.06}TiO_3$.

We also presented results of a LDA+DMFT(QMC) study[48] of the Mott-Hubbard metal-insulator transition (MIT) in the paramagnetic phase of (doped) V_2O_3. These results showed a MIT at a reasonable value of the Coulomb interaction $U \approx 5\,\mathrm{eV}$ and are in very good agreement with the experimentally determined photoemission and X-ray absorption spectra for this system, i.e., above *and* below the Fermi energy. In particular, we find a spin state $S = 1$ in the paramagnetic phase, and an orbital admixture of $e_g^\pi e_g^\pi$ and $e_g^\pi a_{1g}$ configurations, which both agree with recent experiments. Thus, LDA+DMFT(QMC) provides a remarkably accurate microscopic theory of the strongly correlated electrons in the paramagnetic metallic phase of V_2O_3.

Another material where electronic correlations are considered to be important is cerium. We reviewed our recent investigations of the Ce α-γ transition, based on LDA+DMFT(QMC)[60,61] and LDA+DMFT(NCA)[59] calculations. The spectral results and susceptibilities show the same tendency as seen in the experiment, namely a dramatic reduction in the size of the quasiparticle peak at the Fermi level when passing from the α- to the γ-phase. While we do not know at the moment whether the zero-temperature quasiparticle peak will completely disappear at an even larger volume (i.e., in a rather Mott-like fashion) or simply fade away continuously with increasing volume (i.e., in a more Kondo-like fashion), an important aspect of our results is that the rapid reduction in the size of the peak seems to coincide with the appearance of a negative curvature in the correlation energy and a shallow minimum in the total energy. This suggest that the electronic correlations responsible for the reduction of the quasiparticle peak are associated with energetic changes that are strong enough to cause a volume collapse in the sense of the Kondo volume collapse model,[104] or a Mott transition model[103] including electronic correlations.

We also discussed the embedding of LDA+DMFT in a spectral density functional theory, and extensions like self-consistent LDA+DMFT calculations, LDA+cluster DMFT, and GW+DMFT. These extensions are still work in progress which have been applied to model systems or, in the case of self-consistent LDA+DMFT, to Pu where a fast IPT-inspired DMFT solver has been employed.[57,58] A systematic analysis of the effect of these extensions in the context of realistic calculations is still mandatory and certainly depends on the system at hand. E.g., one would

certainly expect the non-local correlations taken into account by cluster DMFT approaches to be much more important for effectively one- and two-dimensional systems than in three dimensions.

Another important aspect of future investigations is the calculation of other physical quantities. In the first LDA+DMFT publications, mainly the local spectral function (Green function) was calculated because it arises naturally in the DMFT self-consistency scheme. Nonetheless, in the near future more physical quantities will be calculated by LDA+DMFT: thermodynamic properties like the specific heat or entropy, which have been already calculated for f-electron systems but not yet for transition metal oxides; transport properties like the electrical, optical, and thermal conductivity; magnetic, orbital and other susceptibilities; calculations will also be performed within symmetry broken phases and phase diagrams will be obtained.

Physicists from two strong solid state communities, i.e., the DFT bandstructure and the many-body community, have finally joined forces to develop and apply LDA+DMFT. The outcome is a powerful tool for future investigations of electronic properties of real materials *with strong electronic correlations*.

Acknowledgments

We are grateful to J. W. Allen, O. K. Andersen, P. W. Anderson, R. Bulla, R. Claessen, U. Eckern, G. Esirgen, A. Georges, K.-H. Höck, S. Horn, M. Jarrell, J. Keller, H.-D. Kim, D. E. Kondakov, G. Kotliar, J. Lægsgaard, A. Lichtenstein, D. van der Marel, W. Metzner, T. M. Rice, G. A. Sawatzky, J. Schmalian, M. Schramme, M. Sigrist, M. Ulmke, and M. Zölfl for helpful discussions. We thank A. Sandvik for making available his maximum entropy code. The QMC code of Ref. 33 App. D was modified for use for some of the results of Section 6. This work was supported in part by the Deutsche Forschungsgemeinschaft through the Emmy-Noether program (KH), Sonderforschungsbereich 484 (DV, GK, VE), Forschergruppe HO 955/2 (VE), and project Pr 298/5-1 & 2 (TP), the Russian Foundation for Basic Research by RFFI-01-02-17063 (VA) and RFFI-02-02-06162 (IN), the U.S. Department of Energy by University California LLNL under contract No. W-7405-Eng-48. (AM), the U.S. National Science Foundation by DMR-9985978 (RS), the Lorentz Center in Leiden and the Kalvi Institute for Theoretical Physics at the University of California, Santa Barbara, for their hospitality and support, the Leibniz-Rechenzentrum, München, and the John v. Neumann-Institut for Computing, Jülich.

References

[1] P. Hohenberg and W. Kohn, Phys. Rev. B **136**, 864 (1964).

[2] W. Kohn and L. J. Sham, Phys. Rev. **140**, 4A, A1133 (1965); W. Kohn and L. J. Sham, Phys. Rev. A - Gen. Phys. **140**, 1133 (1965); L. J. Sham and W. Kohn, Phys. Rev. **145 N 2**, 561 (1966).

[3] R. O. Jones and O. Gunnarsson, Rev. Mod. Phys. **61**, 689 (1989).

[4] T. C. Leung, X. W. Wang, and B. N. Harmon, Phys. Rev. B **37**, 384 (1988); J. Zaanen, O. Jepsen, O. Gunnarsson, A. T. Paxton, and O. K. Andersen, Physica C **153**, 1636 (1988); W. E. Pickett, Rev. Mod. Phys. **61**, 433 (1989).

[5] L. F. Mattheiss, J. Phys.: Cond. Matt. **6**, 6477 (1994).

[6] K. Held, I. A. Nekrasov, G. Keller, V. Eyert, N. Blümer, A. K. McMahan, R. T. Scalettar, Th. Pruschke, V. I. Anisimov, and D. Vollhardt, in *Quantum Simulations of Complex Many-Body Systems: From Theory to Algorithms*, J. Grotendorst, D. Marks, and A. Muramatsu (ed.), NIC Series Volume 10, p. 175-209 (2002).

[7] A. I. Lichtenstein, M. I. Katsnelson, and G. Kotliar, to be published in *Electron Correlations and Materials Properties 2*, A. Gonis (ed.), Kluwer, New York; G. Kotliar and S. Savrasov, in *New Theoretical Approaches to Strongly Correlated Systems*, A. M. Tsvelik (ed.), Kluwer, New York, 2001, p. 259.

[8] M. Born and R. Oppenheimer, Ann. Phys. (Leipzig) **84**, 457 (1927).

[9] M. Levy, Proc. Natl. Acad. Sci. (USA), **76**, 6062 (1979).

[10] L. Hedin and B. Lundqvist, J. Phys. C: Solid State Phys. **4**, 2064 (1971); U. von Barth and L. Hedin, J. Phys. C: Solid State Phys. **5**, 1629 (1972).

[11] D. M. Ceperley and B. J. Alder, Phys. Rev. Lett. **45**, 566 (1980).

[12] O. K. Andersen, Phys. Rev. B **12**, 3060 (1975); O. Gunnarsson, O. Jepsen, and O. K. Andersen, Phys. Rev. B **27**, 7144 (1983); O. K. Andersen and O. Jepsen, Phys. Rev. Lett. **53**, 2571 (1984).

[13] O. K. Andersen, T. Saha-Dasgupta, S. Ezhov, L. Tsetseris, O. Jepsen, R. W. Tank, C. Arcangeli, and G. Krier, Psi-k Newsletter 45, 86 (2001).

[14] E. Müller-Hartmann, Z. Phys. B **74**, 507 (1989); ibid. B **76**, 211 (1989).

[15] J. Wahle, N. Blümer, J. Schlipf, K. Held, and D. Vollhardt, Phys. Rev. B **58**, 12749 (1998).

[16] O. Gunnarson, O. K. Andersen, O. Jepsen, and J. Zaanen, Phys. Rev. B **39**, 1708 (1989).

[17] I. A. Nekrasov, K. Held, N. Blümer, A. I. Poteryaev, V. I. Anisimov, and D. Vollhardt, Euro. Phys. J. B **18**, 55 (2000).

[18] I. Solovyev, N. Hamada, and K. Terakura, Phys. Rev. B **53**, 7158 (1996).

[19] V. I. Anisimov, J. Zaanen, and O. K. Andersen, Phys. Rev. B **44**, 943 (1991); V. I. Anisimov, F. Aryasetiawan, and A. I. Lichtenstein, J. Phys. Cond. Matter **9**, 767 (1997).

[20] V. I. Anisimov, A. I. Poteryaev, M. A. Korotin, A. O. Anokhin, and G. Kotliar, J. Phys. Cond. Matter **9**, 7359 (1997).

[21] A. I. Lichtenstein and M. I. Katsnelson, Phys. Rev. B **57**, 6884 (1998).

[22] V. Drchal, V. Janiš, and J. Kudrnovský, in *Electron Correlations and Material Properties*, edited by A. Gonis, N. Kioussis, and M. Ciftan, Kluwer/Plenum, New York, 1999, p. 273.

[23] J. Lægsgaard and A. Svane, Phys. Rev. B **58**, 12817 (1998).

[24] Th. Wolenski, *Combining bandstructure and dynamical mean-field theory: A new perspective on* V_2O_3, Ph.D. Thesis, Universität Hamburg 1998 (Shaker Verlag, Aachen, 1999).

[25] M. B. Zölfl, Th. Pruschke, J. Keller, A. I. Poteryaev, I. A. Nekrasov, and V. I. Anisimov, Phys. Rev. B **61**, 12810 (2000).

[26] W. Metzner and D. Vollhardt, Phys. Rev. Lett. **62**, 324 (1989).

[27] U. Brandt and C. Mielsch, Z. Phys. B **75**, 365 (1989); ibid. B **79**, 295 (1989); ibid. B **82**, 37 (1991).

[28] V. Janiš, Z. Phys. B **83**, 227 (1991); V. Janiš and D. Vollhardt, Int. J. Mod. Phys. **6**, 731 (1992).

[29] A. Georges and G. Kotliar, Phys. Rev. B **45**, 6479 (1992).

[30] M. Jarrell, Phys. Rev. Lett. **69**, 168 (1992).

[31] D. Vollhardt, in *Correlated Electron Systems*, edited by V. J. Emery, World Scientific, Singapore, 1993, p. 57.

[32] Th. Pruschke, M. Jarrell, and J. K. Freericks, Adv. in Phys. **44**, 187 (1995).

[33] A. Georges, G. Kotliar, W. Krauth, and M. J. Rozenberg, Rev. Mod. Phys. **68**, 13 (1996).

[34] P. W. Anderson, in *Moment formation in solids*, edited by W. J. L. Buyers, Plenum Press, New York and London, 1984, p. 313.

[35] W. Negele and H. Orland, *Quantum Many-Particle Systems*, Addison-Wesley, New York, 1987.

[36] H. Keiter and J. C. Kimball, Phys. Rev. Lett. **25**, 672 (1970); N. E. Bickers, D. L. Cox, and J. W. Wilkins, Phys. Rev. B **36**, 2036 (1987).

[37] Th. Pruschke and N. Grewe, Z. Phys. B **74**, 439 (1989).

[38] Th. Pruschke, D. L. Cox, and M. Jarrell, Phys. Rev. B **47**, 3553 (1993).

[39] J. E. Hirsch and R. M. Fye, Phys. Rev. Lett. **56**, 2521 (1986); M. Jarrell, Phys. Rev. Lett. **69**, 168 (1992); M. Rozenberg, X. Y. Zhang, and G. Kotliar, Phys. Rev. Lett. **69**, 1236 (1992); A. Georges and W. Krauth, Phys. Rev. Lett. **69**, 1240 (1992); M. Jarrell, in *Numerical Methods for Lattice Quantum Many-Body Problems*, edited by D. Scalapino, Addison Wesley, 1997.

[40] M. J. Rozenberg, Phys. Rev. B **55**, R4855 (1997).

[41] J. E. Han, M. Jarrell, and D. L. Cox, Phys. Rev. B **58**, R4199 (1998).

[42] K. Held and D. Vollhardt, Euro. Phys. J. B **5**, 473 (1998).

[43] M. Caffarel and W. Krauth, Phys. Rev. Lett. **72**, 1545 (1994).

[44] R. Bulla, Adv. Sol. State Phys. **46**, 169 (2000).

[45] H. Kajueter and G. Kotliar, Int. J. Mod. Phys. **11**, 729 (1997).

[46] M. I. Katsnelson and A. I. Lichtenstein, J. Phys. Cond. Matter **11**, 1037 (1999).

[47] M. I. Katsnelson and A. I. Lichtenstein, Phys. Rev. B **61**, 8906 (2000).

[48] K. Held, G. Keller, V. Eyert, V. I. Anisimov, and D. Vollhardt, Phys. Rev. Lett. **86**, 5345 (2001).

[49] M. S. Laad, L. Craco, and E. Müller-Hartmann, cond-mat/0211210.

[50] I.A. Nekrasov, G. Keller, D.E. Kondakov, A.V. Kozhevnikov, Th. Pruschke, K. Held, D. Vollhardt, and V.I. Anisimov, cond-mat/0211508; A. Liebsch, cond-mat/0301537.

[51] I.A. Nekrasov, Z.V. Pchelkina, G. Keller, Th. Pruschke, K. Held, A. Krimmel, D. Vollhardt, and V.I. Anisimov, Phys. Rev. B **67**, 85111 (2003).

[52] A. Liebsch and A. I. Lichtenstein, Phys. Rev. Lett. **84**, 1591 (2000); A. Liebsch, cond-mat/0301536.

[53] V. I. Anisimov, I. A. Nekrasov, D. E. Kondakov, T. M. Rice, and M. Sigrist, Eur. Phys. J. B **25**, 191-201 (2002).

[54] L. Craco, M. S. Laad, and E. Müller-Hartmann, cond-mat/0209132.

[55] A. I. Lichtenstein, M. I. Katsnelson, and G. Kotliar Phys. Rev. Lett. **87**, 67205 (2001).

[56] S. Biermann, A. Dallmeyer, C. Carbone, W. Eberhardt, C. Pampuch, O. Rader, M. I. Katsnelson, and A. I. Lichtenstein, cond-mat/0112430.

[57] S. Y. Savrasov, G. Kotliar, and E. Abrahams, Nature **410**, 793 (2001).

[58] S. Y. Savrasov and G. Kotliar, cond-mat/0106308.

[59] M. B. Zölfl, I. A. Nekrasov, Th. Pruschke, V. I. Anisimov, and J. Keller, Phys. Rev. Lett. **87**, 276403 (2001).

[60] K. Held, A. K. McMahan, and R. T. Scalettar, Phys. Rev. Lett. **87**, 276404 (2001).

[61] A. K. McMahan, K. Held, and R. T. Scalettar, Phys. Rev. B **67**, 75108 (2003).

[62] W. Weber, J. Bünemann, and F. Gebhard, in *Band-Ferromagnetism*, edited by K. Baberschke, M. Donath, and W. Nolting, Lecture Notes in Physics, Vol. 580 (Springer, Berlin, 2001), p. 9; J. Bünemann, F. Gebhard, W. Weber, Phys. Rev. B **57**, 6896 (1998).

[63] M. Suzuki, Prog. Theor. Phys. **56**, 1454 (1976)

[64] One limitation of QMC is that it is very difficult to deal with the spin-flip term of the Hund's rule coupling because of a "minus-sign problem" which arises in a Hubbard-Stratonovich decoupling of this spin-flip term, see K. Held, *Untersuchung korrelierter Elektronensysteme im Rahmen der Dynamischen Molekularfeldtheorie*, Ph.D. thesis, Universität Augsburg 1999 (Shaker Verlag, Aachen, 1999). In the particle-hole symmetric case another decoupling scheme which includes the spin-flip term is possible without "minus-sign problem", see Y. Motome and M. Imada, J. Phys. Soc. Jap. **66**, 1872 (1997).

[65] N. Metropolis, A. W. Rosenbluth, M. N. Rosenbluth, A. H. Teller, and E. Teller, J. Chem. Phys. **21**, 1087 (1953).

[66] M. Jarrell and J. E. Gubernatis, Physics Reports **269**, 133 (1996).

[67] E. Müller-Hartmann, Z. Phys. B **57**, 281 (1984).

[68] G. Kotliar, Physica B 259-261, 711 (1999). R. Chitra and G. Kotliar, Phys. Rev. B **62**, 12715 (2000).

[69] R. Fukuda, T. Kotani, and S. Yokojima, Prog. Theory Phys. **92**, 833 (1994); R. Fukuda et al., Prog. Theory Phys. Suppl. **121**, 1 (1996).

[70] G. Kotliar, S. Y. Savrasov, G. Pálsson, and G. Biroli, Phys. Rev. Lett. **87**, 186401 (2001); G. Biroli and G. Kotliar, Phys. Rev. B **65**, 155112 (2002).

[71] A. I. Lichtenstein and M. I. Katsnelson, Phys. Rev. B **62**, 9283 (2000).

[72] M. Potthoff, M. Aichhorn, and C. Dahnken, preprint.

[73] M. H. Hettler, A. N. Tahvildar-Zadeh, and M. Jarrell, Phys. Rev. B **58**, 7475 (1998); M. H. Hettler, M. Mukherjee, M. Jarrell, and H. R. Krishnamurthy, Phys. Rev. B **61**, 12739 (2000). Note, that one of the implementations in Ref. 71 is equivalent to DCA.

[74] A. Schiller and K. Ingersent, Phys. Rev. Lett. **75**, 113 (1995); G. Zaránd, D. L. Cox, and A. Schiller, Phys. Rev. B **62**, 16227 (2000).

[75] Th. Maier, M. Jarrell, Th. Pruschke, and J. Keller, Phys. Rev. Lett. **85**, 1524 (2000); Eur. Phys. J. B **13** 613 (2000); C. Huscroft, M. Jarrell, Th. Maier, S. Moukouri, and A. N. Tahvildarzadeh, Phys. Rev. Lett. **86**, 139 (2001).

[76] L. Hedin, Phys. Rev. **139**, A796 (1965); F. Aryasetiawan and O. Gunnarsson, Rep. Prog. Phys. **61**, 237 (1998).

[77] P. Sun and G. Kotliar, Phys. Rev. B **66**, 85120 (2002); S. Biermann, F. Aryasetiawan, and A. Georges, cond-mat/0207419.

[78] D. A. MacLean, H.-N. Ng, and J. E. Greedan, J. Solid State Chem. **30**, 35 (1979).

[79] M. Eitel and J. E. Greedan, Journal of the Less-Common Metals **116**, 95 (1986).

[80] J. P. Gopel, J. E. Greedan, and D. A. MacLean, J. Solid State Chem. **43**, 244 (1981).

[81] Y. Okimoto, T. Katsufuji, Y. Okada, T. Arima, and Y. Tokura, Phys. Rev. B **51**, 9581 (1995).

[82] W. Heindl, Th. Pruschke, and J. Keller, J. Phys. – Condens. Matter **12**, 2245 (2000).

[83] At present, QMC simulations of the DMFT equations are not feasible at the experimental temperature (80K). We note, however, that no intrinsic temperature dependence was observed in the experiment,[84] at least up to room temperature.

[84] A. Fujimori *et al*, Phys. Rev. Lett. **69**, 1796 (1992). A. Fujimori *et al*, Phys. Rev. B **46**, 9841 (1992). A qualitatively *and* quantitatively similar spectrum was obtained recently by T. Yoshida, A. Ino, T. Mizokawa, A. Fujimori, Y. Taguchi, T. Katsufuji, and Y. Tokura, Europhys. Lett. **59**, 258 (2002), with an experimental energy resolution of only 30 meV. One may suppose, however, that broadening effects due to the polycrystalline nature of the sample and surface effects are, then, larger than the instrumental resolution.

[85] B. Keimer, D. Casa, A. Ivanov, J.W. Lynn, M. v. Zimmermann, J.P. Hill, D. Gibbs, Y. Taguchi, and Y. Tokura, Phys. Rev. Lett. **85**, 3946 (2000).

[86] N. F. Mott, Rev. Mod. Phys. **40**, 677 (1968); *Metal-Insulator Transitions* (Taylor & Francis, London, 1990); F. Gebhard, *The Mott Metal-Insulator Transition* (Springer, Berlin, 1997).

[87] D. B. McWhan *et al.*, Phys. Rev. B **7**, 1920 (1973).

[88] J. Hubbard, Proc. Roy. Soc. London Ser. A **276**, 238 (1963); **277**, 237 (1963); **281**, 401 (1964).

[89] W. F. Brinkman and T. M. Rice, Phys. Rev. B **2**, 4302 (1970).

[90] G. Moeller, Q. Si, G. Kotliar, and M. Rozenberg, Phys. Rev. Lett. **74**, 2082 (1995); J. Schlipf, M. Jarrell, P. G. J. van Dongen, N. Blümer, S. Kehrein, Th. Pruschke, and D. Vollhardt, Phys. Rev. Lett. **82**, 4890 (1999); M. J. Rozenberg, R. Chitra, and G. Kotliar, Phys. Rev. Lett. **83**, 3498 (1999); R. Bulla, Phys. Rev. Lett. **83**, 136 (1999); R. Bulla, T. A. Costi, and D. Vollhardt, Phys. Rev. B **64**, 45103 (2001); J. Joo and V. Oudovenko, Phys. Rev. B **64**, 193102 (2001); N. Blümer, *Mott-Hubbard Metal-Insulator Transition and Optical Conductivity in High Dimensions*, Ph.D. thesis, Universität Augsburg 2002.

[91] P. D. Dernier, J. Phys. Chem. Solids **31**, 2569 (1970).

[92] Use of the crystal structure of Cr-doped V_2O_3 for the insulating phase of pure V_2O_3 is justified by the observation that Cr-doping is equivalent to the application of (negative) pressure.

[93] M. Schramme, Ph.D. thesis, Universität Augsburg 2000 (Shaker Verlag, Aachen, 2000); M. Schramme *et al.* (unpublished).

[94] S.-K. Mo, J. D. Denlinger, H.-D. Kim, J.-H. Park, J. W. Allen, A. Sekiyama, A. Yamasaki, K. Kadono, S. Suga, Y. Saitoh, T. Muro, P. Metcalf, G. Keller, K. Held, V. Eyert, V. I. Anisimov, and D. Vollhardt, cond-mat/0212110.

[95] O. Müller, J. P. Urbach, E. Goering, T. Weber, R. Barth, H. Schuler, M. Klemm, S. Horn, and M. L. denBoer, Phys. Rev. B **56**, 15056 (1997).

[96] J.-H. Park, L. H. Tjeng, A. Tanaka, J. W. Allen, C. T. Chen, P. Metcalf, J. M. Honig, F. M. F. de Groot, and G. A. Sawatzky, Phys. Rev. B **61**, 11 506 (2000).

[97] D. J. Arnold and R. W. Mires, J. Chem. Phys. **48**, 2231 (1968).

[98] C. Castellani, C. R. Natoli, and J. Ranninger, Phys. Rev. B **18**, 4945 (1978); **18**, 4967 (1978); **18**, 5001 (1978).

[99] M. J. Rozenberg, G. Kotliar, H. Kajueter, G. A. Thomas, D. H. Rapkine, J. M. Honig, and P. Metcalf, Phys. Rev. Lett. **75**, 105 (1995).

[100] *Handbook on the Physics and Chemistry of Rare Earths*, edited by K. A. Gschneider Jr. and L. R. Eyring (North-Holland, Amsterdam, 1978); in particular, D. G. Koskenmaki and K. A. Gschneider Jr., *ibid*, p.337.

[101] J. S. Olsen, L. Gerward, U. Benedict, and J.-P. Itié, Physica **133B**, 129 (1985).

[102] A. K. McMahan, C. Huscroft, R. T. Scalettar, and E. L. Pollock, J. Comput.-Aided Mater. Design **5**, 131 (1998).

[103] B. Johansson, Philos. Mag. **30**, 469 (1974); B. Johansson, I.A. Abrikosov, M. Aldén, A. V. Ruban, and H.L. Skriver Phys. Rev. Lett. **74**, 2335 (1995).

[104] J. W. Allen and R. M. Martin, Phys. Rev. Lett. **49**, 1106, (1982); J. W. Allen and L. Z. Liu, Phys. Rev. B **46**, 5047, (1992); M. Lavagna, C. Lacroix, and M. Cyrot, Phys. Lett. **90A**, 210 (1982).

[105] K. Held, C. Huscroft, R.T. Scalettar, and A.K. McMahan, Phys. Rev. Lett. **85**, 373 (2000); see also C. Huscroft, A. K. McMahan, and R. T. Scalettar, Phys. Rev. Lett. **82**, 2342 (1999).

[106] K. Held and R. Bulla, Eur. Phys. J. B **17**, 7 (2000).

[107] We solve self-consistently for n_f using a $4f$ self energy $\Sigma = U_f(n_f - \frac{1}{2})$, and then remove this contribution from the eigenvalue sum to get the kinetic energy. The potential energy is taken to be $\frac{1}{2}U_f n_f(n_f - 1)$.

[108] L. Z. Liu, J. W. Allen, O. Gunnarsson, N. E. Christensen, and O. K. Andersen, Phys. Rev. B **45,** 8934 (1992).

[109] A. P. Murani, Z. A. Bowden, A. D. Taylor, R. Osborn, and W. G. Marshall, Phys. Rev B **48,** 13981 (1993).

[110] D. M. Wieliczka, C. G. Olson, and D. W. Lynch, Phys. Rev. B **29,** 3028 (1984).

[111] E. Wuilloud, H. R. Moser, W. D. Schneider, and Y. Baer, Phys. Rev. B **28,** 7354 (1983).